Master's Thesis

Unanticipated Mechanism of the Trimethylsilyl Motif in Electrolyte Additives on Nickel-Rich Cathodes in Lithium-Ion Batteries

Min Woo Park

Department of Energy Engineering
(Battery Science and Technology)

Ulsan National Institute of Science and Technology

2021

Unanticipated Mechanism of the Trimethylsilyl Motif in Electrolyte Additives on Nickel-Rich Cathodes in Lithium-Ion Batteries

Min Woo Park

Department of Energy Engineering
(Battery Science and Technology)

Ulsan National Institute of Science and Technology

ULSAN NATIONAL INSTITUTE OF SCIENCE AND TECHNOLOGY

Unanticipated Mechanism of the Trimethylsilyl Motif in Electrolyte Additives on Nickel-Rich Cathodes in Lithium-Ion Batteries

A thesis/dissertation
submitted to the Graduate School of UNIST
in partial fulfillment of the
requirements for the degree of
Master of Science

Min Woo Park

12/18/2020

Approved by

Advisor
Nam-Soon Choi

ULSAN NATIONAL INSTITUTE OF SCIENCE AND TECHNOLOGY

Unanticipated Mechanism of the Trimethylsilyl Motif in Electrolyte Additives on Nickel-Rich Cathodes in Lithium-Ion Batteries

Min Woo Park

This certifies that the thesis/dissertation of Min Woo Park is approved.

12/18/2020

Signature

Advisor: Nam-Soon Choi

Signature

Kyeong-Min Jeong

Signature

Sung You Hong

Abstracts

Various electrolyte additives containing trimethylsilyl (TMS) motif have been reported to remove HF formed by the decomposition of $LiPF_6$-based electrolyte and suppress dissolving transition metal from the cathode in Li-ion batteries (LIBs). Among them, tris(trimethylsilyl)phosphite (TMSP) was used as a multi-functional additive that increases the cycle performance of LIBs by forming a stable cathode electrolyte interphase (CEI) layer by decomposing before the electrolyte as well as scavenging HF which present in electrolytes. However, we found that TMSP-containing electrolyte exhibited poor performance compared to baseline electrolyte that does not have a TMS motif on 80% Ni-containing $LiNi_xCo_yMn_zO_2$ (NCM) electrodes. At this, we compared the cycle performance of TMSP-containing electrolyte using not only NCM electrode with 80% Ni content but also 60% electrode and $LiCoO_2$ (LCO) cathode with 80% nickel content. In addition, we propose the causes and mechanism of deterioration of additives with TMS motifs using NMR, SEM, and TEM analysis.

Contents

List of figures

Figure 14. Spectra of ^{31}P NMR the (a) DMC with 2 wt % TMSP additive and (b) DMC with 2 wt % TMPi additive which added 2.5 wt % residue lithium species (LiOH/ Li_2CO_3). (c) TMSP decomposition caused by LiOH residual lithium (d) Anticipated reaction mechanisms on carbonate-based solvents through TMSOH produced from the chemical reaction in TMSP and LiOH.

Figure 15. Spectra of ^{11}B NMR of DMC with 2 wt % TMSB added 2.5 wt % LiOH/Li_2CO_3.

Figure 16. ^{19}F and ^{31}P NMR spectra of 1 M $LiPF_6$ in EC/EMC/DMC (2/4/4, volume %) (a) absence and presence (b) with 1 wt % TMSOH stored after 24h. (c) Anticipated chemical reactions with TMSOH and TMSF, POF_3 and HF which produced from PF_5.

Figure 17. 1H NMR spectra of the (a) TMSOH in the DMC and (b) 2 wt % TMSP + 2.5 wt % LiOH in DMC after storage for 24 h at 25 °C.

Figure 18. During 150 cycles (a) Cyclic performance, (b) cell Coulombic efficiency, and (c) capacity retention of NCM811/graphite full cells presence and absence 0.5 wt % TMSOH at 25 °C (charge and discharge rates: 1C).

Figure 19. ^{19}F NMR spectra of 2 M $LiPF_6$ in EC/EMC/DMC (2/4/4, vol %) (Ref) presence and absence 1.5 wt % TMSOH before storage (fresh) and after storage for 10 h at 25 °C in the ranges (a) -90 – -80 ppm, (b) -170 – -150 ppm and (c) -200 – -180 ppm.

Figure 20. (a) Leakage current plot for Li|NCM811 half-cells at a constant voltage of 4.4 V vs. Li/Li+. (b) Comparison of EIS from the NCM622 and NCM811 with graphite anode after pre-cycle. Differential capacity profiles (dQ/dV plots) for NCM811/graphite anode full cells with the (c) baseline and (d) 0.5 wt % TMSP-containing electrolyte during charging. The dQ/dV plots are presented for selected cycle numbers (1st and 2nd cycles and every 10 cycles) for 200 cycles.

Figure 21. STEM images of the 200 cycled NCM811 cathodes (a) not containing and (b) containing 0.5 wt % TMSP with FFT image. 520 eV – 550 eV range of EELS spectra of (c) baseline and (d) 0.5 wt % TMSP-containing electrolyte. (e) 3D depth TOF-SIMS images for species that P-, PO2-, PO2F2- and LiF2- ions of NCM811 cathodes of baseline electrolyte and with 0.5 wt % TMSP electrolyte.

Figure 22. XRD analysis data of the pristine NCM811 cathode and 200 cycled NCM811 cathodes with and without 0.5 wt % TMSP additive in the following 2θ ranges: (a) 10–80°, (b) 10–50°, (c) 37.5–39°, and (d) 63–67°.

Figure 23. XPS spectra for C 1s, F 1s and P 2p of (a) 200 cycled NCM811 cathodes cycled in baseline electrolytes and 0.5 wt % TMSP-containing electrolyte. O 1s, F 1s and P 2p of (b) 200cycled graphite anodes cycled in baseline electrolyte and 0.5 wt % TMSP.

List of table

1. Introduction

1.1. Principles Lithium-ion battery

Lithium ion battery (LIB) is kind of rechargeable battery that lithium ions transfer from the cathode to the anode through the charging, and are in the spotlight as an energy storage device with great energy density and operating voltage and no memory effect.

Lithium ion battery consists of cathode material, anode material, electrolyte and separator, and cathode active material is the most significant constituents for determining the capacity of a battery (Figure 1). Cathode such as $LiCoO_2$ (LCO) and $LiNi_xCo_yMn_zO_2$ (NCM111), which were widely used up to this time, showed excellent rate property or stability. However, these cathode materials have limitations that cannot achieve the high energy density required by the growing power grid/utility-energy storage systems (ESS), electric vehicles (EV) and electronic mobile devices (Table 1). To attain high gravimetric and volumetric energy, high capacity high nickel (Ni) oxide ($LiNi_{1-x-y}Co_xMn_yO_2$, $1-x-y \geq 0.8$) is measured as the main materials for great energy density lithium-ion batteries. When Ni content is 60% ($1-x-y = 0.6$), the cathode can produce 170mAh/g, but when Ni content increases to 80% ($1-x-y = 0.8$), the cathode can produce 200mAh/g or more. [1]–[5]

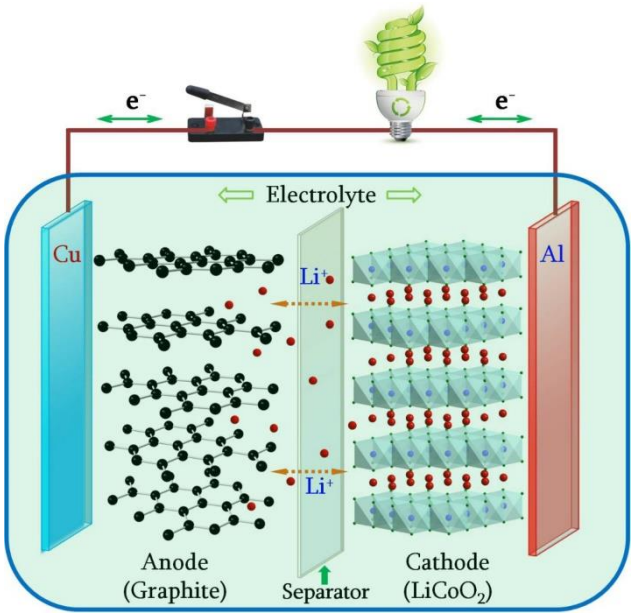

Figure 1. Schematic of the commercialized secondary LIB. [6]

Material	Structure	Potential vs. Li/Li^+, (Average V)	Specific Capacity, (mAh/g)	Specific Energy, (Wh/kg)
$LiCoO_2$ (LCO)	Layered	3.9	140	546
$LiNi_{0.8}Co_{0.15}Al_{0.05}O_2$ (NCA)	Layered	3.8	180-200	680-760
$LiNi_{1/3}Co_{1/3}Mn_{1/3}O_2$ (NCM)	Layered	3.8	160-170	610-650
$LiMn_2O_4$ (LMO)	Spinel	4.1	100-120	410-492
$LiFePO_4$ (LFP)	Olivine	3.45	150-170	518-587

Table 1. Characteristics of Commercial LIB cathode active materials. [7]

1.2. High nickel cathode problems and improvement plan

High nickel cathode shows reversible capacity exceeding 210 mAh/g at a charge voltage of 4.3V versus Li/Li^+, but suffers from harmful phase transition compared to Li/Li^+ at 4.0V and above. The oxidation of H3-phase lattice oxygen results in irreversible O_2 evolution from the cathode material and serious structural breakdown of cathode particles occurs. [8]–[13] Moreover, because the Ni^{2+} ion is transferred into the Li slab and the radius of Li^+ and Ni^{2+} is similar, a cation mixture occurs in which the location conversion of Ni^{2+} and lithium ion takes place. Lithium ions thus cannot re-intercalation to the ordinary position through the prolonged cycle, resulting in capacity decay, mechanical degradation and thermal weakness. [14]–[17] Lithium species, which forms near the surface of the cathode, is very easy to react with H_2O, CO or CO_2 in the air, so lithium residue such as Li_2O, LiOH and Li_2CO_3 are generated on the cathode materials surface. [18] These residual lithium cause uneven SEI layer by unanticipated chemical reactions with electrolyte solvents, and the gelation occurs, increasing the pH of the cathode slurry, which causes electrode failure. [16], [17], [19]–[23] Washing process and surface coating were considered to overcome the negative effects of lithium residue paper on high nickel cathode materials. [23]–[25] However, these strategies have not fully addressed the degradation of high nickel cathode occurred by lithium residue species. [23], [26], [27] The cleaning process reduced the amount of lithium in a high nickel cathode structure and also diminished the amount of lithium on the cathode surface. [28] The building of the expected cathode electrode interphase (CEI) layer by cathode electrolyte additives can make performance improvement of high nickel cathode while solving the problem related to residual lithium compounds.

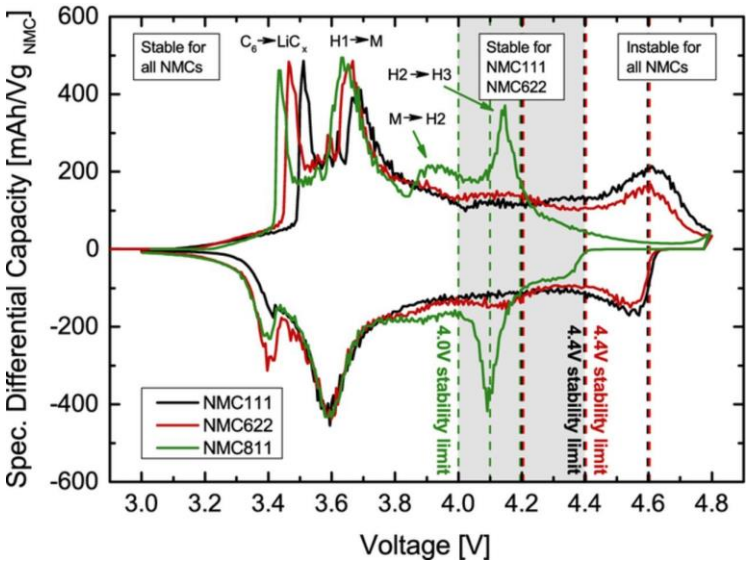

Figure 2. Charge and discharge dQ/dV plot of three kinds of NCM cathodes with graphite anode full-cells with notated phase transformations. [29]

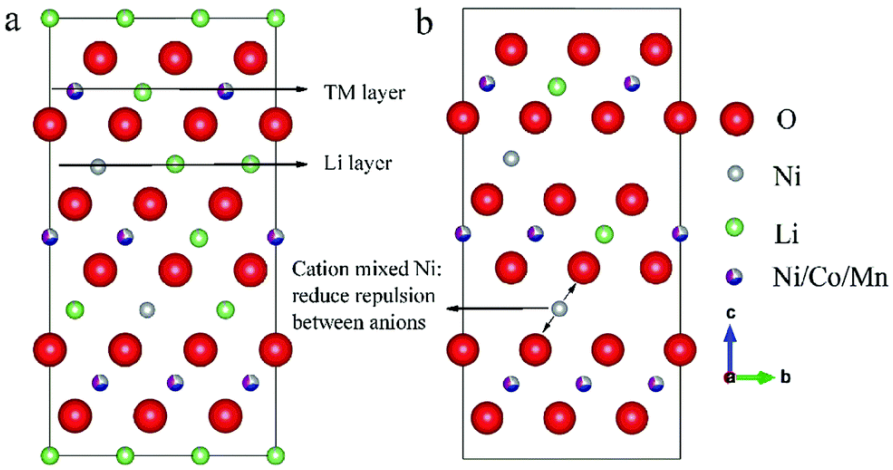

Figure 3. Cation mixed Ni^{2+} maintaining its physical structure during lithiation and delithiation. [30]

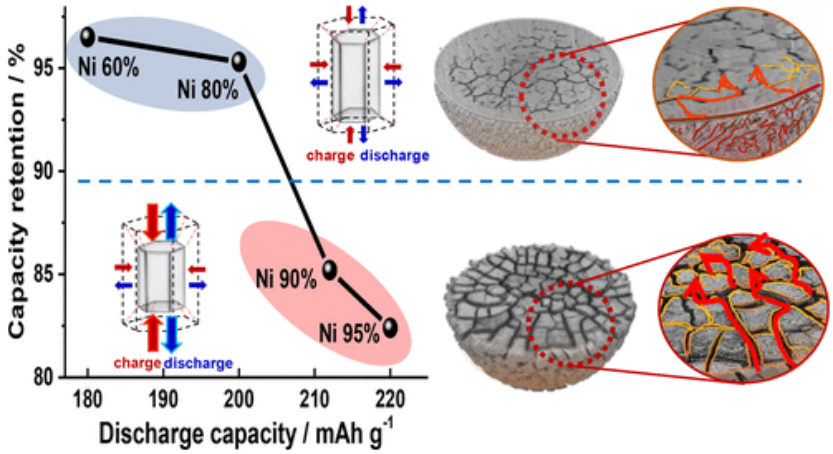

Figure 4. Capacity retention according to nickel content and microcracking on High nickel cathode. [31]

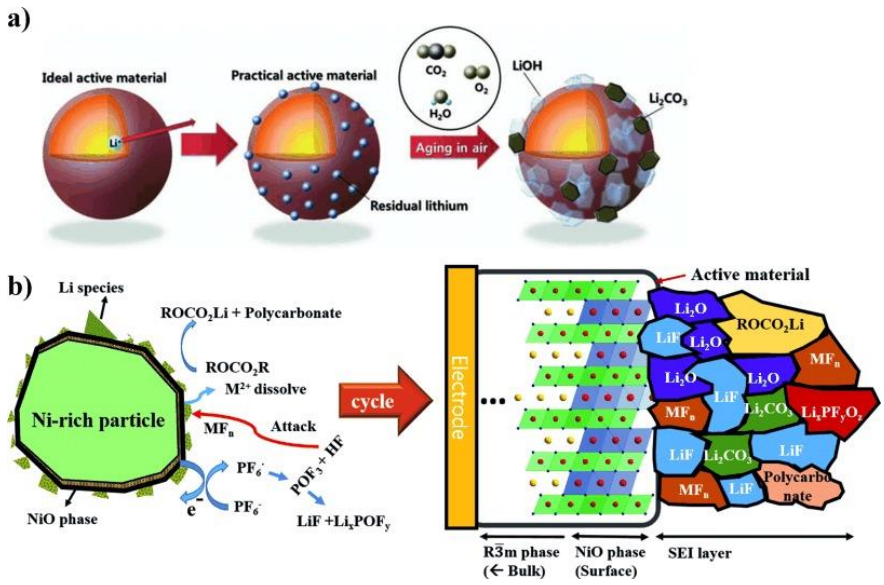

Figure 5. (a) Schematic of the transformation of high-nickel cathode material surface materials in the atmosphere. (b) The configuration of the film layer of the high-nickel cathode surface. [32]

1.3. Apply TMSP electrolyte additive to High nickel cathode

Through the various electrolyte additives, tris(trimethylsilyl) phosphate (TMSP) with good electron donation properties helps form CEI, which is inevitably produced by reaction with H_2O of the $LiPF_6$ usually selected in electrolytes components in LIB, protecting the cathode surface from attacks from HF. [33], [34] Silicon in trimethylsilyl (TMS) functional group of TMSP has a high effect of reducing the acidity of electrolyte in response to fluorine anions of HF, reducing the solubility of conversion metals, and decreasing the resistance lithium fluoride quality (LiF) of CEI. In addition, phosphorus (III) structure of phosphate products can react with harmful HF overreactions forming P=O based compounds and phosphate-HF derivatives, and through reduced reactivity of POF_3, various acids, such as H_2PO_3F and HPO_2F_2, can be produced through further hydrolysis. The TMS group added to the newly prepared $LiPF_6$ electrolyte was considered to have no negative effect on battery cycle performance.

In this paper, we indicate important things of the degradation of the role of expected TMS functional group in high nickel NCM811 cathode combined with anode which is graphite. A relative experiment of phosphite structure and boron-centered (B-core) comparatives with or non-TMS moieties in high nickel (NCM622 and NCM811) is led to inspect whether integrating TMS motifs into additives is useful method to ensure high performance of high nickel Ni-based cathode. The compatibility of TMS moiety with high nickel cathode is detected through electron microscopy, X-ray photoelectron spectroscopy, transmission electron microscopy, flight time secondary ion mass analysis, etc. Finding the function of additives existence of TMS moiety helps to build a stable interface layer that extends the life of the LIB with the High nickel cathodes and functional additive motifs that can clean unwanted HF.

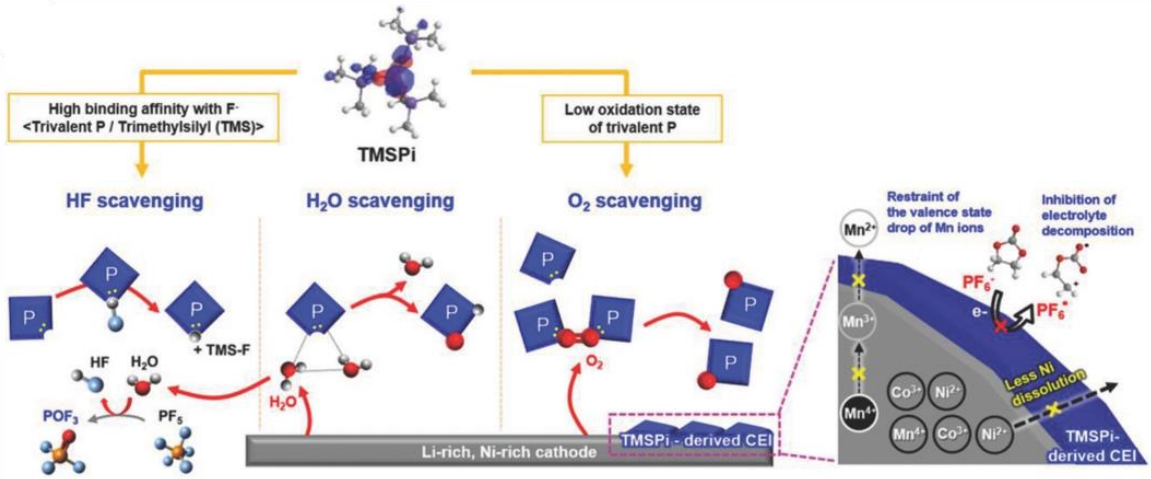

Figure 6. HF, O_2, H_2O scavenging process and function of CEI layer formed by TMSP. [35]

2. Experimental

2.1. Sample preparation

Two types of Ni-rich layered oxide cathodes were used for the electrochemical evaluation of full cells coupled with graphite anodes (namely, $LiNi_{0.6}Co_{0.2}Mn_{0.2}O_2$ (NCM622)|graphite and $LiNi_{0.8}Co_{0.1}Mn_{0.1}O_2$ (NCM811)|graphite). NCM622 was prepared by mixing 92.5 wt % NCM622 as the active material, 4.5 wt % conducting materials (3 wt % carbon black (C65) + 1.5 wt % graphite (SFG6L)) and 3 wt % poly (vinylidene fluoride) (PVDF, Solef 5130) binder. The graphite anode coupled with the NCM622 cathode was composed of 96.6 wt % artificial graphite (S360) as the active material, 1 wt % artificial graphite (S360) as the conducting material and 2.5 wt % binder (1.4 wt % styrene-butadiene rubber (SBR, BM-451B, Zeon Co., Ltd.) and 1 wt % sodium carboxymethyl cellulose (CMC, MAC-350H, Nippon Paper Industries Co., Ltd.). The NCM811 cathode was composed of 94 wt % NCM811, 3 wt % carbon black (Super P) and 3 wt % PVDF (KF9300). The artificial graphite anode (SG17) coupled with the NCM811 cathode was composed of 95 wt % as the active material, 1 wt % carbon black (Super P) as the conducting material, and 4 wt % binder (2 wt % SBR and 2 wt % CMC). The mass loadings of the cathode and graphite were as follows: NCM622 (18 mg cm^{-2})|graphite (8.3 mg cm^{-2}) and NCM811 (10.2 mg cm^{-2})|graphite (7.1 mg cm^{-2}). The baseline electrolyte presented that 1 M $LiPF_6$ dissolved in a mixture of ethylene carbonate (EC), ethyl methyl carbonate (EMC) and dimethyl carbonate (DMC) (2/4/4, vol %) solvent with 1 wt % vinylene carbonate (VC). All solvents and salt were purchased from Soulbrain Co., Ltd. Additive-containing electrolytes were prepared by introducing 0.5 wt % TMSP (Sigma Aldrich, >95%), tris(trimethylsilyl) phosphate (TMSPa, Sigma Aldrich, >98%), tris(trimethylsilyl) borate (TMSB, Sigma Aldrich, >99%) or trimethylphosphite (TMPi, Sigma Aldrich, >99%) to the baseline electrolyte. All the electrolytes were confirmed to contain less than 10 ppm of water by Karl Fischer titration (C20, Mettler Toledo).

2.2. Electrochemical testing

The prolonged cyclic test of NCM cathode material such as NCM622 or NCM811 and LCO was performed using 2032 coin cells. The separator, which is 20 mm thick and 38% porous, was employed. Galvanostatic cycles of the entire cell consist of the cathode and graphite were tested between 2.7V and 4.3V at 25°C (WBCS 3000). The entire cell was cycled at C/10, standard cycling at C/5 for 3 cycles at 25 °C, and 1C for the following cycling with the same temperature condition. For NCM622 and NCM811, 1C matches to 185 mAh/g and 200 mAh/g, one-to-one. To examine the amount of leakage current of the electrolyte containing TMSP in the cathode, the half-cell NCM811 was conducted at 4.4V versus Li/Li^+.

2.3. Characterization

The residual electrolyte was rinsed from the electrode sample using DMC for post-analysis. The differences between composition of the solid electrolyte interphase (SEI) after the TMSP and the unused 200 cycles were confirmed by the flight time secondary ion mass spectrometry (TOF-SIMS) at pressures below 1.1 x 10^{-9} mbar using a pulse 25 keV Bi^{+} primary beam of 1 pA. The results gained by TOF-SIMS were standardized by dividing the entire sum for standardization. A rectangular with a zone of 100 μm x 100 μm was perceived by deepness. A configuration of elements in the surface of electrode was identified by XPS (ThemoFisher, K-Alpha, hν = 1486.6 eV), which is investigating the substance. After 200 cycles test, electrodes and electrodes for XPS were set in sealed Al pouches in glove boxes and rapidly loaded to the XPS device. To check the additional reaction of TMSP with residue species, Li_2CO_3 or LiOH which was purchased by Sigma Aldrich was mixed to DMC as TMSP. The solution was stored for 24 hours at 25°C. After that, ^{31}P NMR spectroscopy was conducted after filtration of the solution (400MHz, Bucker Avance 3HD). Tetrahydrofuran (THF)-contains d8 NMR solvents. Sectional samples for micro-cracking observation of NCM811 cathode were processed by the ion milling method (Hitachi IM4000). [36] Furthermore, the structural change of NCM811 was detected by STEM (JEM-2100Fm JEOL). Electronic energy loss spectrophotometric measurements were made to examine the transformation in the cathode structure with the valence state of Mn, Ni and Co. VSP-300 Galvanostats and potentistat were used to measure total cell impedances. The exact amount of lithium residue species formed on NCM cathode surface was detected by potentiometer titrator (888 Titrando).

3. Results and Discussion

3.1. Characteristics of additives with TMS moiety and degradation in High nickel cathode

Figure 7a shows the chemical structure of organic phosphoric compounds and organoborone compounds with or without highly affinity TMS groups for HF to react Si-F bonds. [37], [38] The combination of Si atoms and O_2 atoms in TMSP, TMSPa and TMSB additive is greatly decomposed by the reaction among TMS functional group and HF (Figure 7b). In Figure 7b, the phosphorus (III) atoms of phosphoric acid compounds such as TMSP and TMPi act as removing HF that occurs the SEI and CEI attack and the make resistant film through reactions with lithium ions. Another unexpected result of HF on cycle performance is that metal ions are decomposed from cathode to electrolyte by HF attacks. [39] Figure 8 shows that TMS motifs in TMSP, TMSPa and TMSB easily capture fluorine anions in HF. Comparing the comparative peak area (x) of HF for the intensity of internal reference additive (C_6F_6) shows that TMSP has strong reactivity than TMSB and TMSPa for HF. Comparison between TMS-containing additives for NCM811 cathode capable of achieving great energy LIB was studied in the battery system of NCM811|graphite. Cells with non-TMSP electrolyte presented 88.6% Coulombic efficiency (CE) after pre-cycling, and 86.4% diminished capacity retention when cycling for 200 cycles. TMPi which has not TMS functional group maintained a discharge capacity of 85.3% similar when using the reference electrolyte. But, with TMS functional group comparatives showed a significant capacity dissipation in the entire cell when cycling was repeated (Figure 7d-f). Furthermore, the addition of TMSP and TMSPa provided poorer discharge capacities (194.8 mAh/g and 194.2 mAh/g) compare to baseline electrolyte (197.9 mAh/g) after pre-cycling. The existence of TMS functional group is likely to have caused this phenomenon because the electrochemical reversibility of the entire cell is not maintained.

The addition of the TMSB gave rise to great potential during pre-cycling, causing the poorest capacity at the discharge of 191.6 mAh/g in the middle of the test comparatives (Figure 7c). Great potentials may be typically related to slow decomposition from NCM811 material and lithography to graphite anode. We estimated the TMSB produced high resistance SEI that interfered with the transmission of charges at graphite anode with NCM811 cathode. Determining the effects of TMS functional group on cycle ability by High nickel cathode, cycle tests of High nickel oxide cathode with a content of 60%, 80% and with an electrolyte of 0.5 wt % TMSP were conducted. TMSP addition of $LiNi_{0.6}Mn_{0.2}Co_{0.2}O_2$(NCM622)|graphite cells reached 89.1% capacity rate with a high CE of 89.1%, 99.5% higher than the retention rate obtained using the reference electrolyte (86.2%).

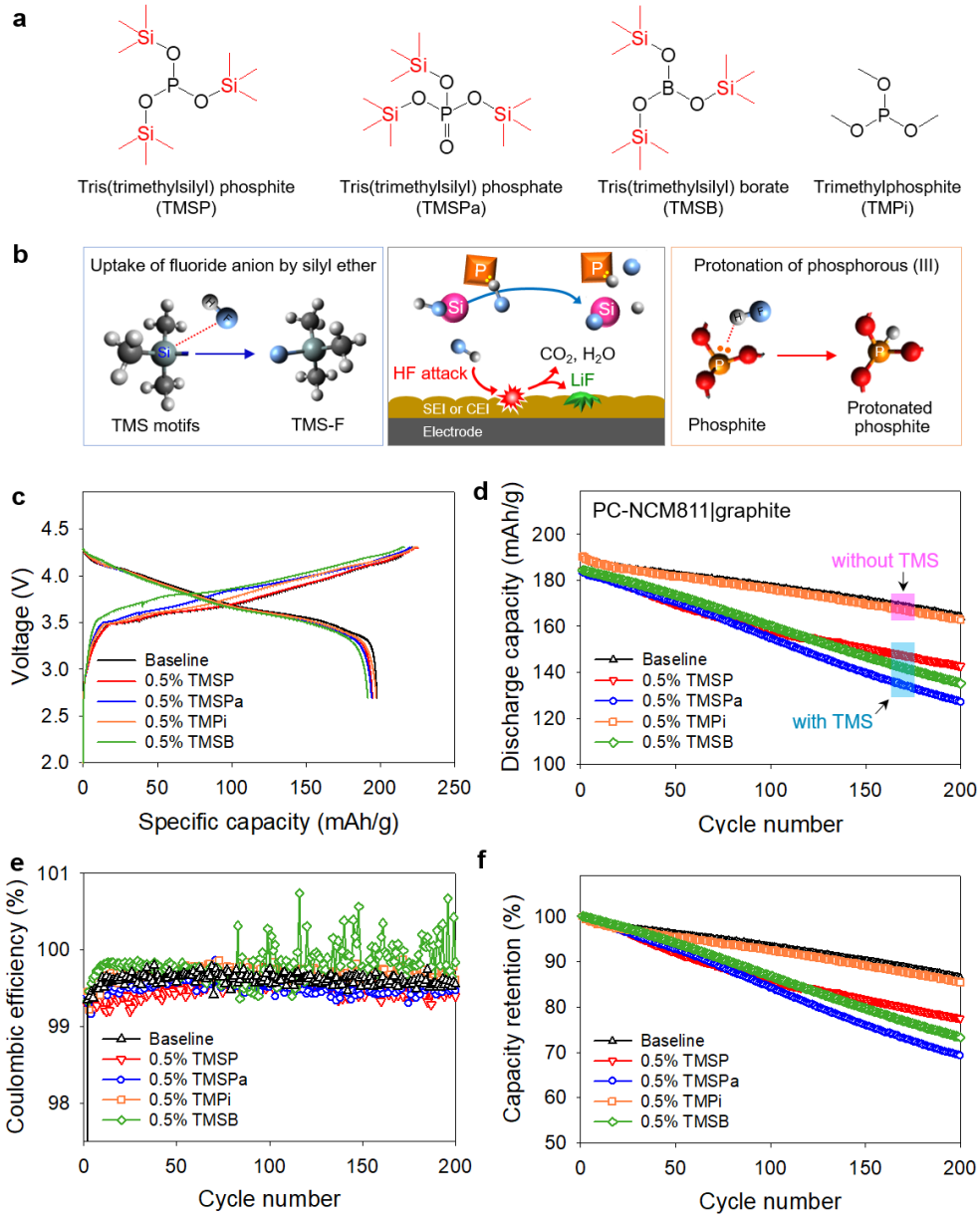

Figure 7. Molecular structures of four additives (a) TMSP, TMSPa, TMSB and TMPi. (b) The expected effect of TMSP electrolyte additive: HF removal through TMS functional group and phosphite structure (c) Voltage profiles of NCM811/graphite during pre-cycling and (d) cyclic performance of NCM811/graphite (e) Coulombic efficiency and (f) capacity retention in NCM811/graphite cell system.

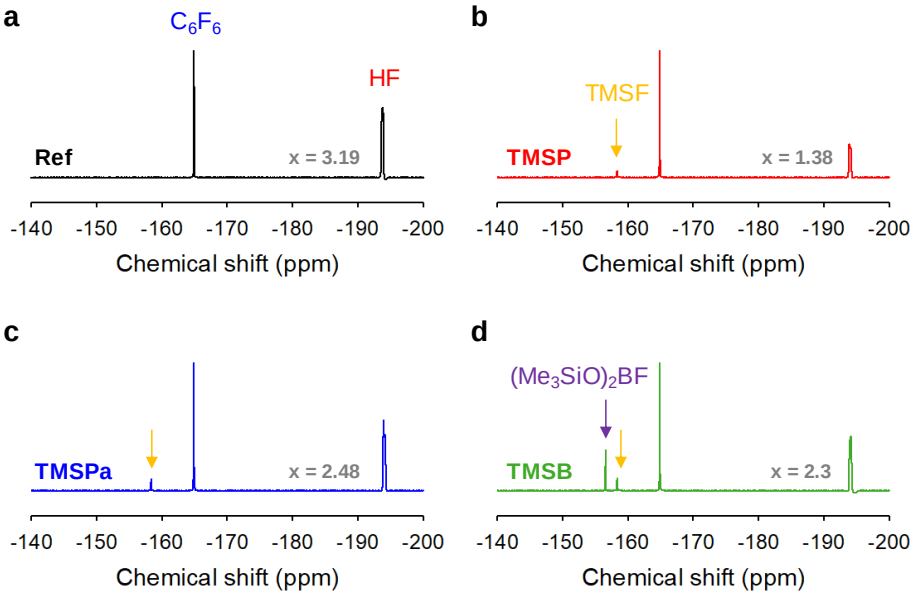

Figure 8. ^{19}F NMR spectra of (a) 1 M $LiPF_6$ in EC/EMC/DMC (2/4/4, vol %) + 1 wt % water (Ref) and addition of the electrolytes, (b) 0.5 wt % TMSP, (c) 0.5 wt % TMSPa, and (d) 0.5 wt % TMSB in 1 M $LiPF_6$ and EC/EMC/DMC (2/4/4, vol %) + 1 wt % water stored for 24 h at 25 °C. The x value is obtained by comparing the integral intensity of the internal reference C_6F_6 and HF.

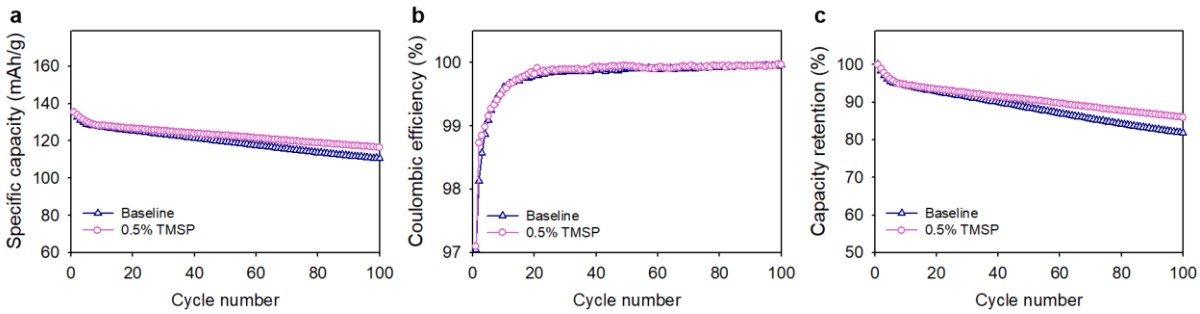

Figure 9. During 100 cycles (a) cyclic performance, (b) cell Coulombic efficiency, and (c) capacity retention of $LiCoO_2$/graphite full cells presence and absence 0.5 wt % TMSP

3.2. TMSP performance difference according to cathode type

$LiCoO_2$ (LCO)/graphite containing TMSP additive electrolyte did not record cycle performance degradation (Figure 9a). In addition, in Figure 9b,c, better CE and capacity of discharge were obtained from electrolytes containing TMSP. The results showed that TMSP does not degrade the capacity retention of LCO with a small amount of LiOH content in the entire active material. However, when cycling for 200 cycles, TMSP produced severe capacity failures and un-uniform CEI of NCM811 and provided disappointing retention of 77.3%, which is poorer than the total cell (86.4%) absence of TMSP (86.3%) (Figure 10b,d). The charging and discharging voltage graphs for 200 cycles are presented in Figure 11. Obviously, using of NCM811/graphite full cell has brought about a severe drop of the voltage plateau with continuous cycles compared to the entire cell without TMSP, representing the negative effect of TMSP on NCM811 cathode. Contrary, the middling discharge voltage plateau remained about 3.7V for the entire cell with an NCM622/graphite at 0.5% TMSP (Figure 11a,b). It might be considered that the amount of residue species of the high-nickel NCM increases with its contents. The most noticeable difference between NCM622 and NCM811 cathode was 1700 ppm of NCM622 and 4190 ppm of NCM811 as the amount of LiOH. In Figure 10e,f the flight time secondary ion mass spectrometry (TOF-SIMS) showed a bright area present to LiOH and Li_2CO_3 in NCM811 cathode. The results show that the NCM811 cathode contains a huge amount of lithium residue species. However, NCM622 cathode presented a comparatively low content of LiOH and Li_2CO_3 in cathode due to comparatively un-strong OH^- and CO_3^- peak intensity. NCM622 at 1700 ppm LiOH undergo unwanted decomposition of TMSP (Figure 12). TMSP did not participate in the reaction with residual lithium which constructs in CEI at the cathode. CEI derived from TMSP mitigated continuous electrolyte decomposition and reduced micro-cracking of NCM622 cathode. The increased content of LiOH in NCM811 particles was combined by primary particles of hundreds of nanoscale size and caused reactions with PF_5 produced by the self-analytical decomposition of $LiPF_6$ (Figure 12b). In Figure 12b, this reaction reinforced the production of HF that attacked SEI and CEI during repetitive cycling. Even worse still, it is possible that the LiOH of NCM811 occurred the decomposition of TMSP to produce TMSOH and insoluble compound Li_3PO_4.

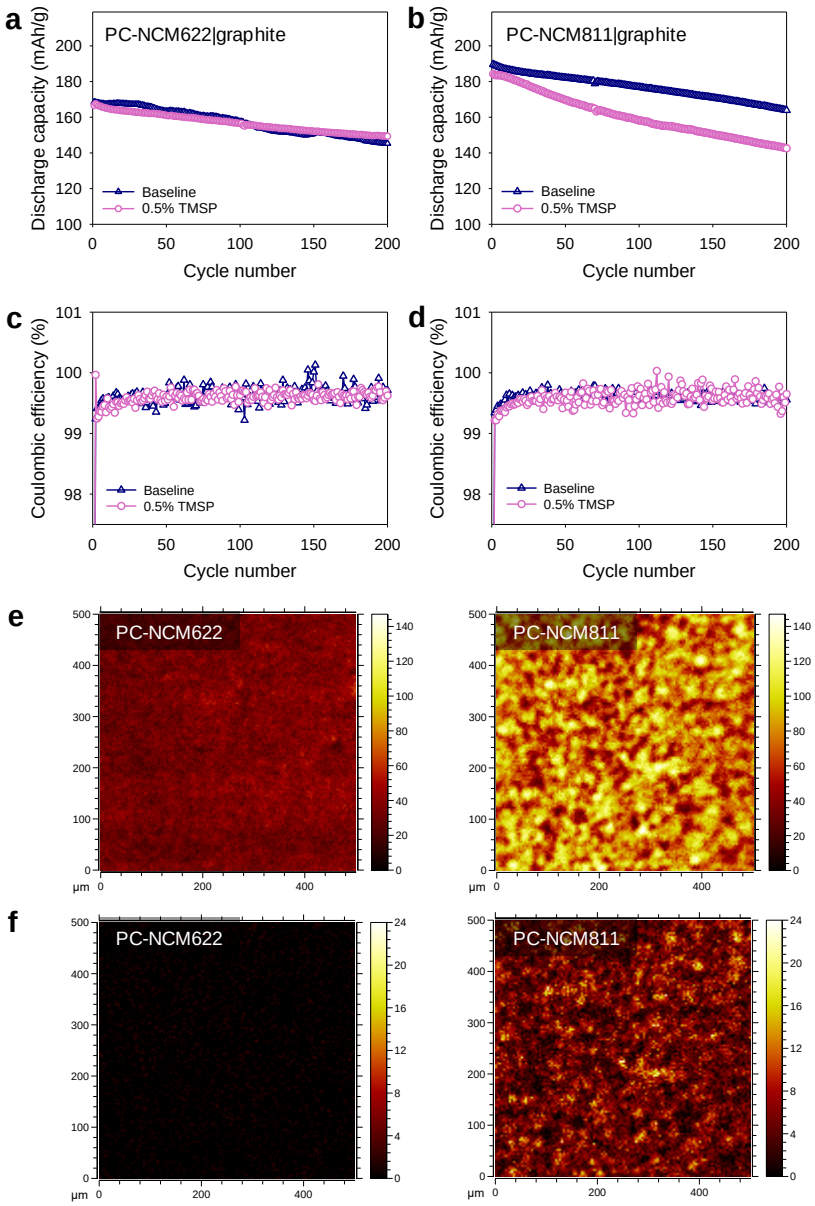

Figure 10. (a,c) Electrochemical cycle test of NCM622/graphite and (b,d) NCM811/graphite. 2D TOF-SIMS images of surface mapping of the pristine cathode. The intensity of (e) OH^- and (f) CO_3^- which presented in the NCM622 or NCM811 electrode.

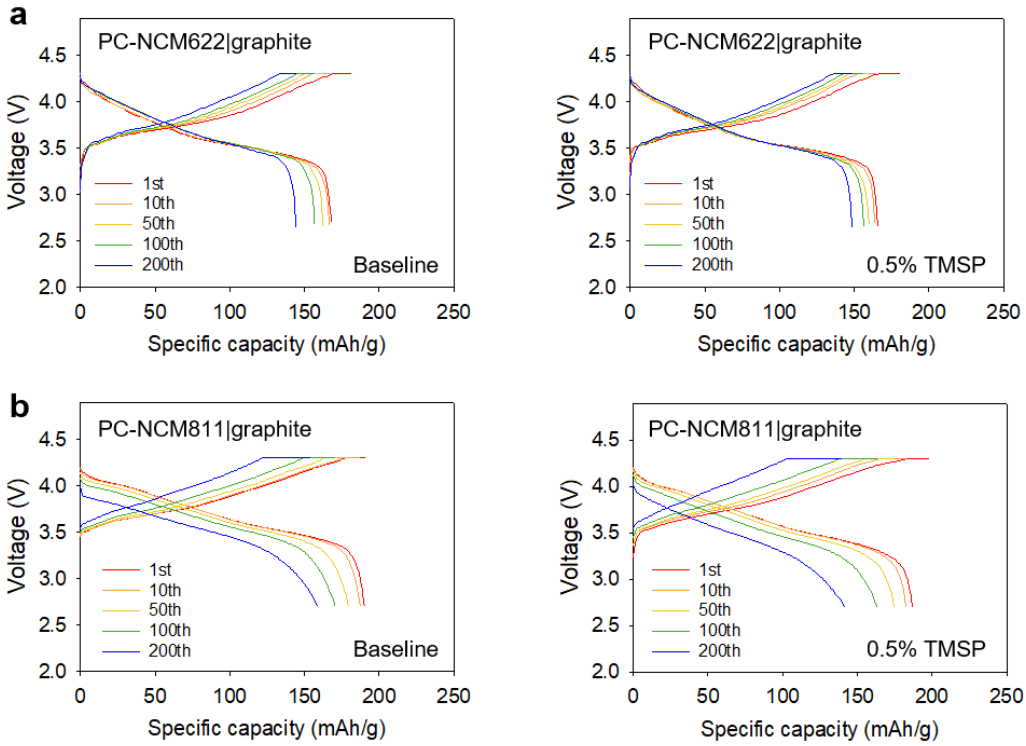

Figure 11. Voltage profiles of full cells that consist of (a) NCM622/graphite and (b) NCM811/graphite by cycles (1st, 10th, 50th, 100th, and 200th cycle) in the baseline electrolyte and 0.5 wt % TMSP-added electrolyte.

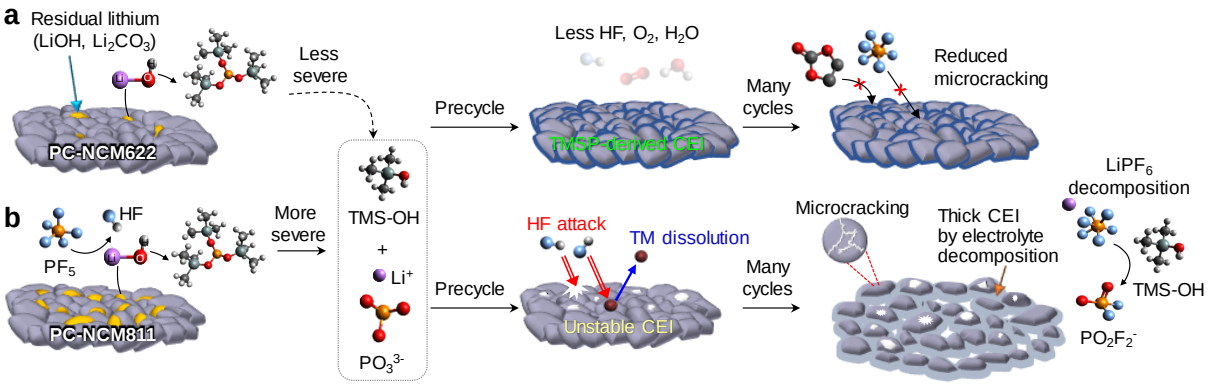

Figure 12. Schematic of overall effects of using TMSP in NCM622 and NCM811.

The LiOH-occurred decomposition of TMSP interfered with the net function of TMSP to construct uniform CEI to ensure cathodic stability. [40] On the NCM811 positive surface, un-uniform CEI did not protect from HF, exacerbated the disassembly of the dissolving TM and produced inhomogeneities in the levels of charging and discharging among the cathode particles. As a result, NCM811 active material with TMSP suffered irreversible stress-induced micro-crack (Figure 13a,b). NCM811 The electrolyte diffusion into a micro-crack of secondary particles continues unwanted decomposition of electrolyte in cathode materials and byproduct causes electrical disconnections between cathode particles. Different from TMSP electrolytes that triggered severe micro-crackers, in the baseline electrolyte, micro-cracks of NCM811 cathode was not severe after pro-longed cycles (Figure 13d,e). In Figure 13c,f, NCM811 cathode had a relatively greater thickness of 0.5wt% TMSP (46.6 mm) than that of cathode using baseline electrolyte (45.3 μm). In addition, uneven CEI formed by TMSP-contained electrolytes may worsen structure conversion (H2 → H3) for the NCM811 cathode.

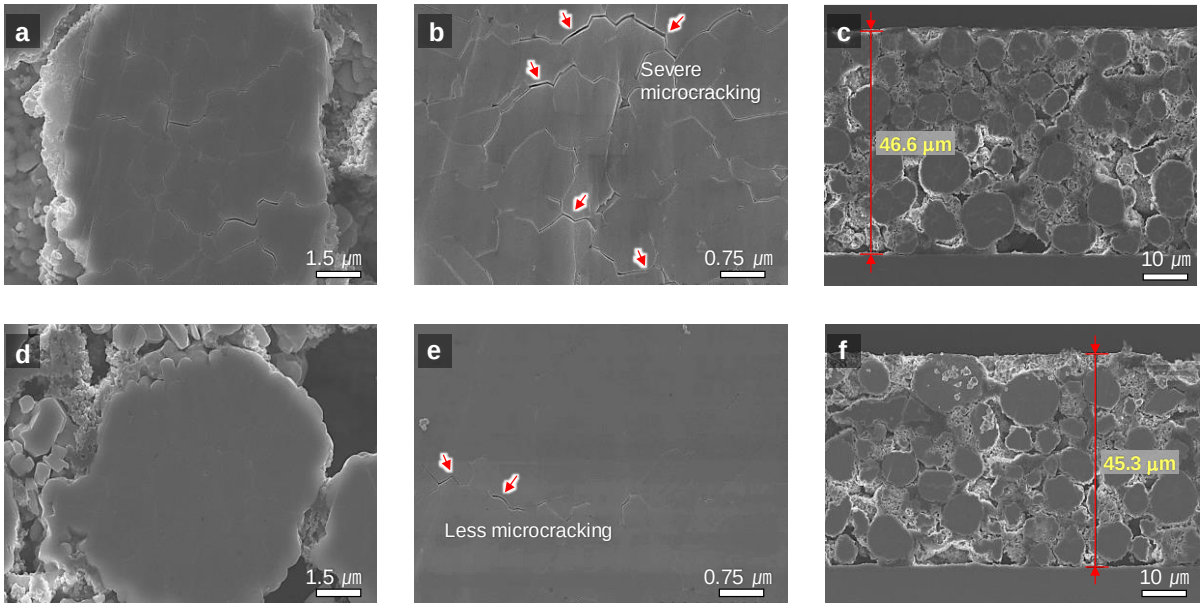

Figure 13. Cross-sectioned SEM images of NCM811 cathodes with (a,b,c) 0.5 wt % TMSP-added electrolyte and (d,e,f) baseline after 200 cyclic test.

3.3. Proposed mechanism of TMSP decomposition by residual lithium

The influence of TMS functional group reaction between phosphite structure containing residue lithium species was examined by NMR study, and residual lithium which is LiOH and Li_2CO_3 was used to DMC solvent with TMSP additive and DMC solvent with TMPi additive, and the subsequent solution was stored for 24 hours. The TMSP peak, which was clearly visible in a solution without residual lithium, looked the same when Li_2CO_3 was added, but the TMSP peak completely disappeared when LiOH was added at 113.9 ppm (Figure 14a). [41] TMSP with non-maximum phosphatase (III) is liable to react with an oxygen molecule to produce a stable phosphate compound of TMSPa. [42] Due to the high degeneration of TMSP, it forms bis(trimethylsilyl)phosphite ($(TMSO)_2PHO$) by reacting with the moisture of DMC solvent. This substance reacts with moisture and oxygen again to form $(TMSO)_2OPO^-$ and ($(TMSO)_2OPOPO(TMSO)_2$). [41], [43], [44] Especially TMSPa in PO_4 detected around -13.6 ppm, $(TMSO)_2PHO$ at 7.56 ppm and ($(TMSO)_2OPOPO(TMSO)_2$) at -24.9 ppm which does not discovered when TMSP with LiOH solution. It is the reason why the electron-like TMS served as a receptor for OH^- in LiOH mixed to DMC with TMSP. Moreover, TMSP is mostly converted to TMSOH, so there is no peak in the spectrum corresponding to LiOH, an insoluble compound such as Li_3PO_4. This phenomenon is the same in TMSB with LiOH solution (Figure 15). However, when using TMPi additive in DMC solution, the TMPi peak does not change adding residual lithium LiOH or Li_2CO_3 (Figure 14b). TMPi is an additive that does not have a TMS group. Comparing the data of the ^{31}P NMR could be incidental with TMS moiety in TMSP additive that has chemical reaction with LiOH, a residual species of the high-nickel cathode. The possible responses between TMSP with LiOH include the production of TMSOH and Li_3PO_4 and may experience additional reactions with an oxygen molecule, as shown in Figure 14c. The TMSOH hydrolyzed PF_5 produced from the self-analytical decomposition of $LiPF_6$ and generate HF, and the sensitive molecule POF_3 produced by the reaction of TMSOH and PF_5 may induce deterioration DMC and EMC which is linear carbonate solvents in the electrolyte.

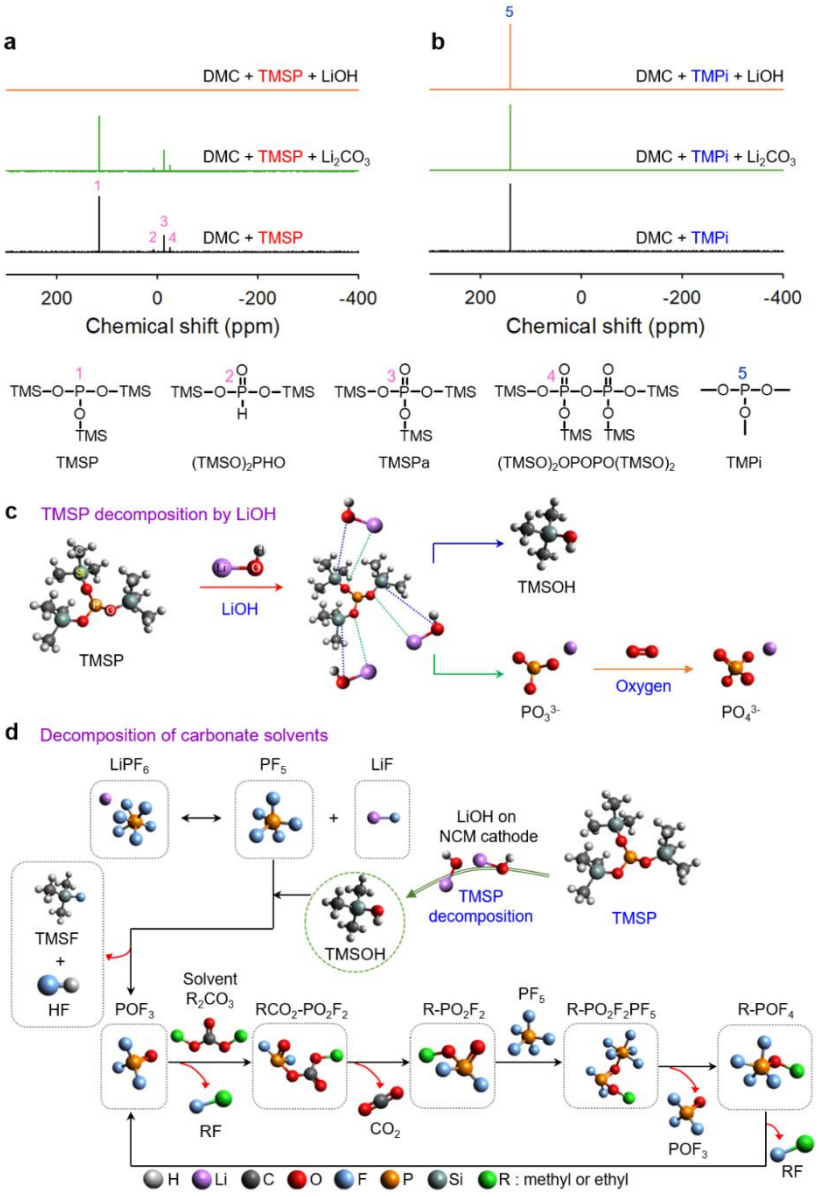

Figure 14. Spectra of ^{31}P NMR the (a) DMC with 2 wt % TMSP additive and (b) DMC with 2 wt % TMPi additive which added 2.5 wt % residue lithium species (LiOH/ Li_2CO_3). (c) TMSP decomposition caused by LiOH residual lithium (d) Anticipated reaction mechanisms on carbonate-based solvents through TMSOH produced from the chemical reaction in TMSP and LiOH.

To deep understand the response between the TMS moiety fixed in high nickel cathodes and LiOH, an ^{11}B NMR study of DMC with 2 wt % tris (trimethylsilyl) borate (TMSB) adding LiOH or Li_2CO_3 was conducted (Figure 15). A peak due to 18.5 ppm of TMSB of DMC + TMSB solution was not detected in LiOH because the TMS group of TMSB responded with OH in LiOH. The reaction with H_2O of $LiPF_6$ salt-induced by TMSOH is figured in Figure 16 of 1 M $LiPF_6$ in EC/EMC/DMC (2:4:4, volume %) measurements of ^{19}F and ^{31}P NMR, added or unadded TMSOH when being stored for 24 h. The marked double peak was -75.3 ppm and -74.0 ppm due to PF_6 anions was shown (Figures 16a,b). Generally, $PO_2F_2^-$ is produced in response to a small amount of water in PF_5. [45], [46] Interestingly, strong peaks of -84.0 ppm and -85.9 ppm allocated to $PO_2F_2^-$ were noticed in the addition of TMSOH (Fig. 16c). It is possible that $PO_2F_2^-$ was generated in response to the creation of TMSOH and the formation of TMSF (Trimethylfluoroide, TMSF) with PF_5. In addition, signals corresponding to the TMSF formed by responses from PF_5 and TMSOH were detected for 1 M $LiPF_6$ in EC/EMC/DMC (2:4:4, volume %) at 1 wt % of TMSOH (2/4/4, volume %) (Figure 16b). Figure 17 shows how TMSOH progresses in TMSP. In DMC, a spectrum of TMSOH is delivered to identify the formation of TMSOH by the chemical reaction between LiOH and TMSP (Figure 17a). ^{1}H NMR analysis showed that 2 wt % of TMSP was completely transformed to TMSOH and hexamethyl disiloxane (TMSOTMS) with 2.5 wt % LiOH at the DMC solution (Figure 17b). [40], [47] It confirms that LiOH aggressively decomposes TMSP during TMSOH generation. Obviously, the reaction between LiOH and TMSP on NCM811 (Figure 12b) ends up in the disappointment role of TMSP.

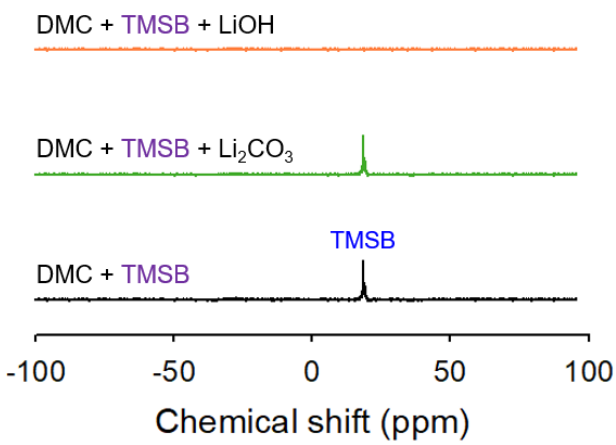

Figure 15. Spectra of ^{11}B NMR of DMC with 2 wt % TMSB added 2.5 wt % LiOH/Li_2CO_3.

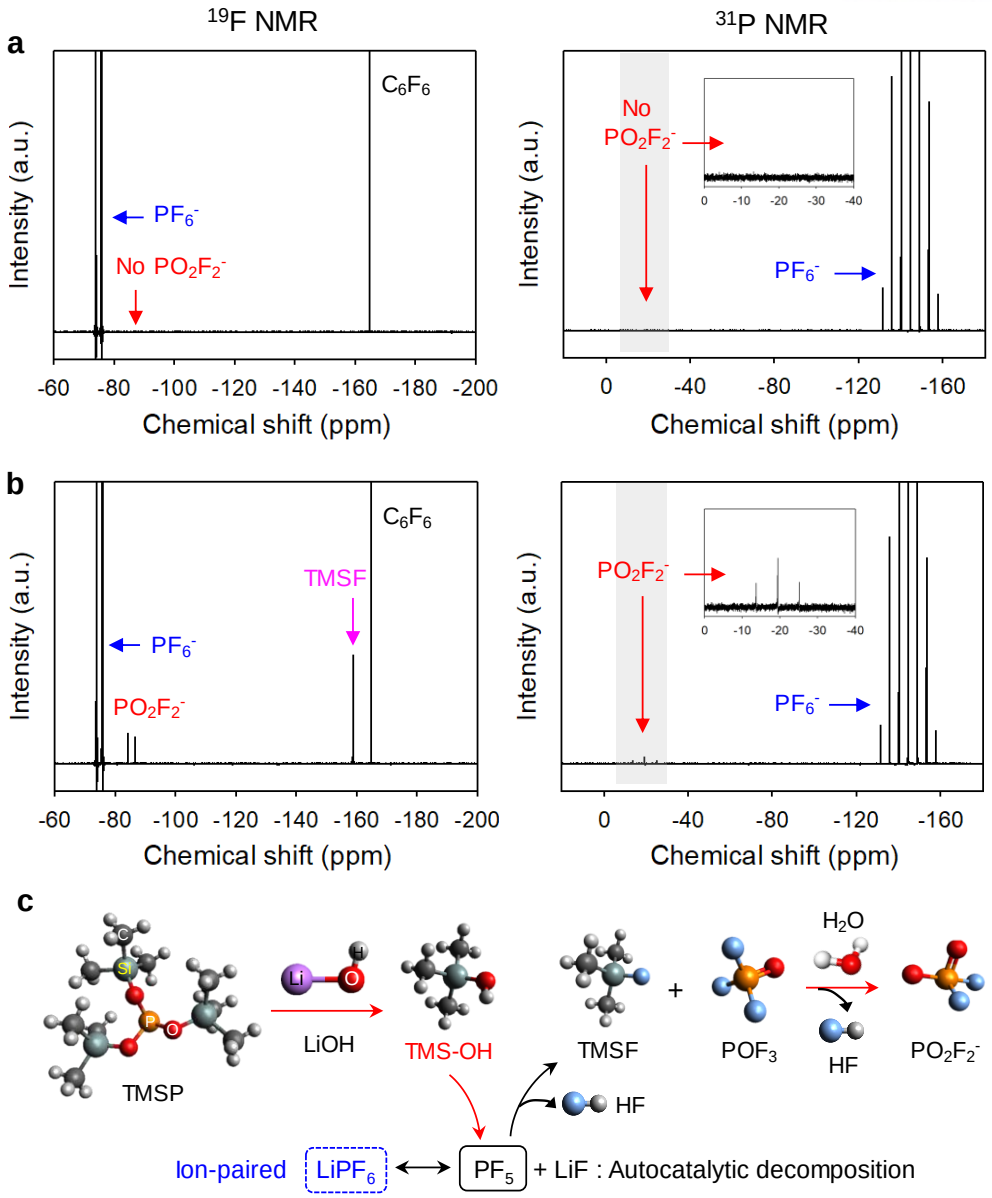

Figure 16. ^{19}F and ^{31}P NMR spectra of 1 M $LiPF_6$ in EC/EMC/DMC (2/4/4, volume %) (a) absence and presence (b) with 1 wt % TMSOH stored after 24h. (c) Anticipated chemical reactions with TMSOH and TMSF, POF_3 and HF which produced from PF_5.

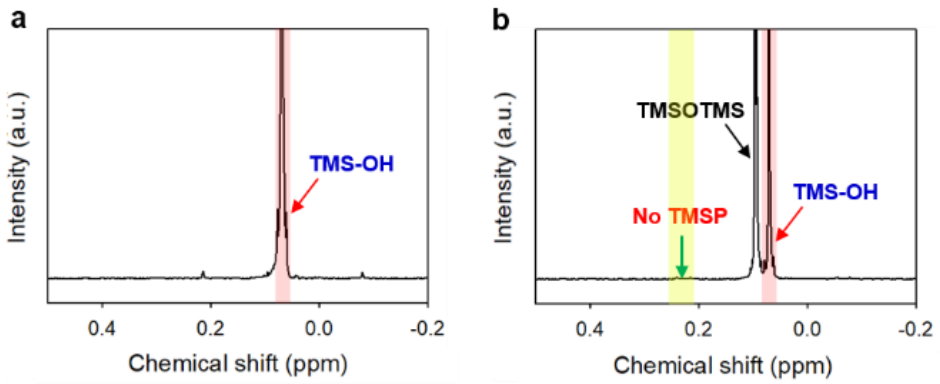

Figure 17. ^{1}H NMR spectra of the (a) TMSOH in the DMC and (b) 2 wt % TMSP + 2.5 wt % LiOH in DMC after storage for 24 h at 25 °C.

Additional verification of the undesirable effects of TMSOH is detected through a relative experiment of the cycling performance of the full cell consisting of graphite anodes of 0.5 wt % TMSOH and NCM811 cathode (Figure 18). In TMSOH-added electrolyte induced generating of HF by hydrolysis of $LiPF_6$, which dissolving of transition metal from NCM material and attacking the film of electrodes, resulting in lower cycle stability compared to that obtained using reference electrolytes. TMSF peak -158.6 ppm shows that HF produced from an electrolyte containing $LiPF_6$ can be removed when using TMSOH (Figure 19). In Figure 20a, adding TMSP had a bad effect on the oxidation stability of electrolytes. The rise in the oxidation current of the TMSP means that unrepairable electrolyte damage of 4.4V versus Li/Li^+ occurred at NCM811 cathode, and permanent damage of CEI occurred. This ununiformed Ni-rich cathode with TMSP additive is supposed to reduce the cycle performance of Ni-rich cathode combined with a graphite anode. Furthermore, TMSP makes a resistive interface (insulating layer (R_i) + charge-transfer resistance (R_{ct}) of CEI and SEI) in NCM811 surface (Figure 20b). Due to the high reactivity of TMSP to LiOH, an uneven surfactant layer was developed for the NCM811 cathode, thus accumulating resistive by-products inside the NCM811 cathode, destroying secondary cathode particles. It also shows a resistive film has been built on NCM811 cathode in TMSP-containing electrolyte. The phase conversion range at about 4.25V (H2 + H3 phase), which added to the structural deformation of Ni-rich cathode, enlarged significantly for NCM811|graphite in TMSP-containing electrolyte (Fig.20c,d) during charging. Clearly, TMSP strengthened unstable H3 phase formation, inducing micro-crack of NCM811 cathode.

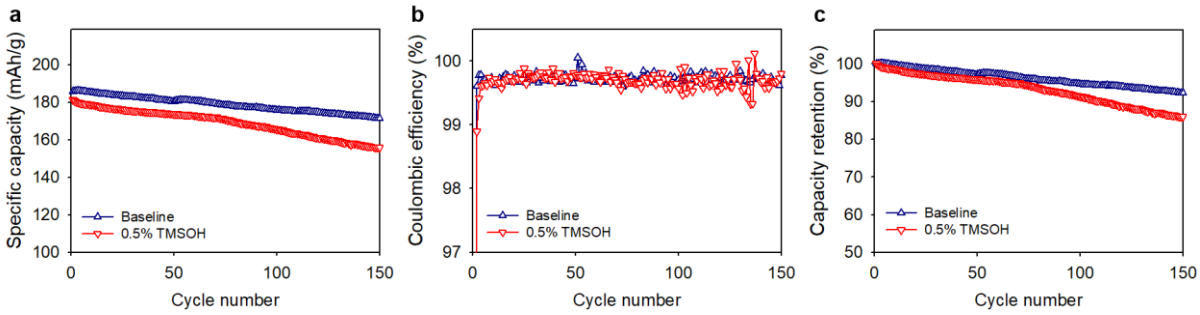

Figure 18. During 150 cycles (a) Cyclic performance, (b) cell Coulombic efficiency, and (c) capacity retention of NCM811/graphite full cells presence and absence 0.5 wt % TMSOH at 25 °C (charge and discharge rates: 1C).

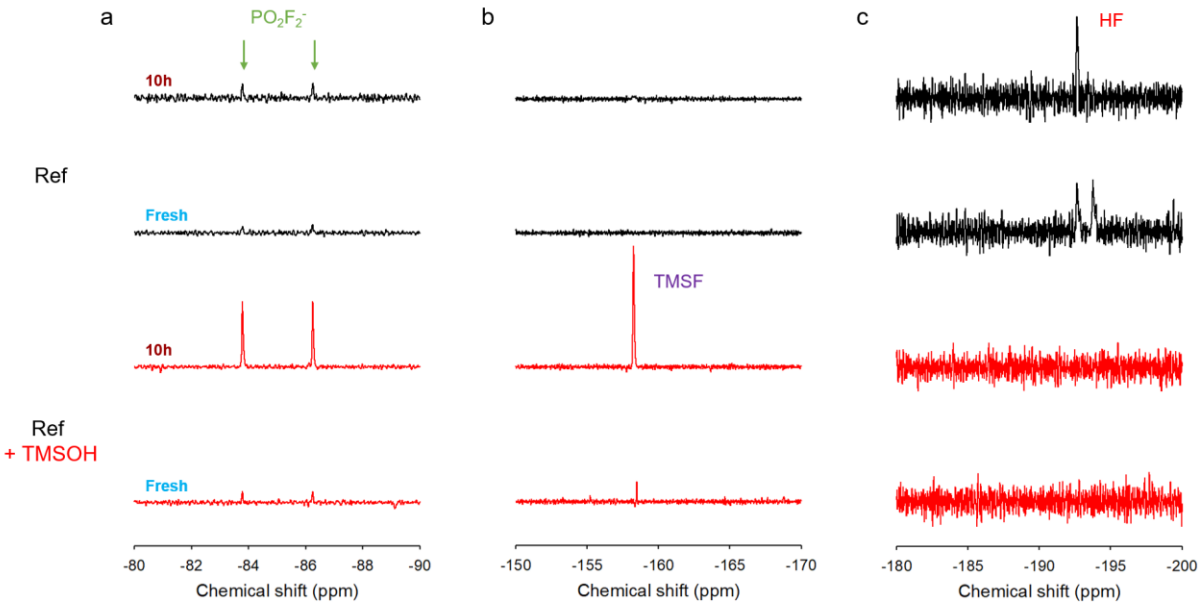

Figure 19. ^{19}F NMR spectra of 2 M $LiPF_6$ in EC/EMC/DMC (2/4/4, vol %) (Ref) presence and absence 1.5 wt % TMSOH before storage (fresh) and after storage for 10 h at 25 °C in the ranges (a) -90 – -80 ppm, (b) -170 – -150 ppm and (c) -200 – -180 ppm.

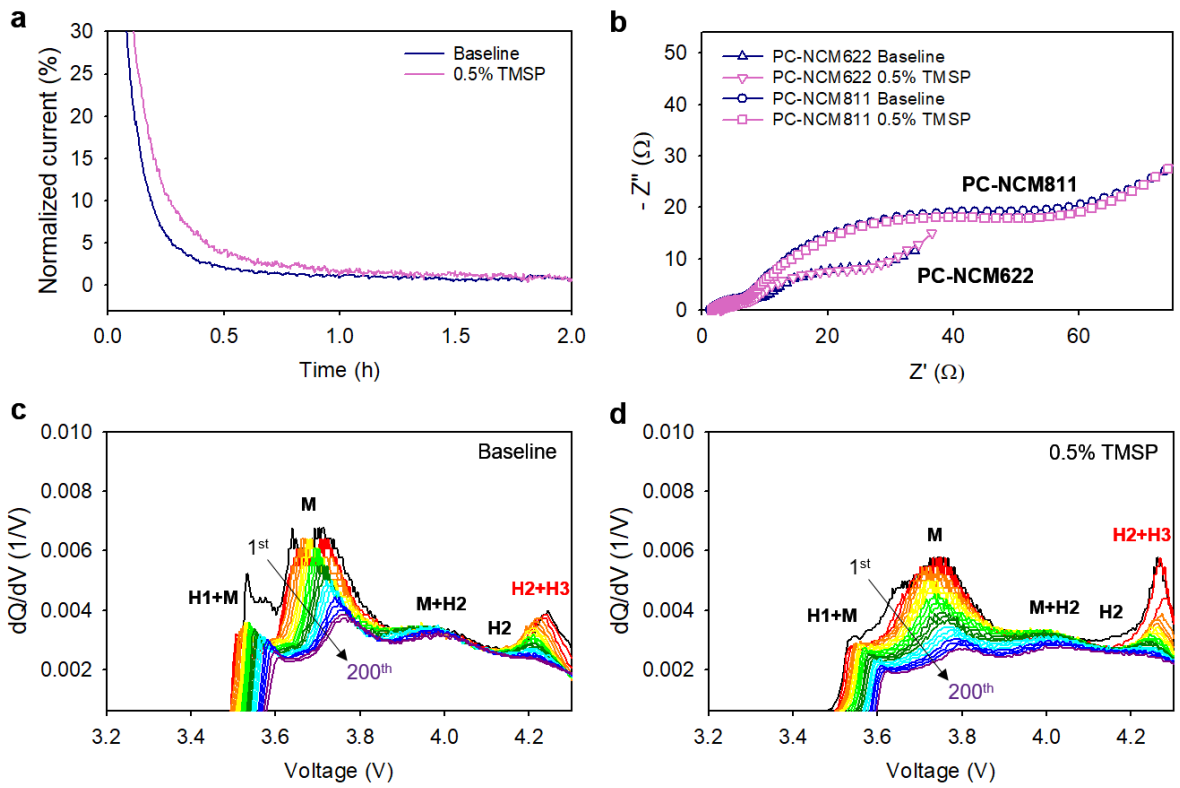

Figure 20. (a) Leakage current plot for Li|NCM811 half-cells at a constant voltage of 4.4 V vs. Li/Li^{+}. (b) Comparison of EIS from the NCM622 and NCM811 with graphite anode after pre-cycle. Differential capacity profiles (dQ/dV plots) for NCM811/graphite anode full cells with the (c) baseline and (d) 0.5 wt % TMSP-containing electrolyte during charging. The dQ/dV plots are presented for selected cycle numbers (1st and 2nd cycles and every 10 cycles) for 200 cycles.

3.4. Analysis of degradation

The harmful effects of TMSP on NCM811 cathode were revealed through a transmitting electron microscope (STEM) image. In addition, fast Fourier transform (FFT) analysis supports them (Fig. 21a,b). The phase conversion to electrochemical inert rock-salt (NiO like) phase occurred in large quantities of NCM811 on the surface. In Figure 21a, STEM images and FFT patterns show that NCM811 cathode baseline electrolyte NiO like phase (A area) about 2.8nm and a clear-layered structure (B area) remaining detection part. The rock-salt area was greatly converted to 7.6 nm with electrolyte to which TMSP was added, and Ni-O like phase (C area) and layered structure (D area) were identified by FFT pattern. The EELS results support the degradation when using TMSP additive on the phase transition of NCM811 cathode. [48], [49] The clear peak at about 529 eV indicates the gap between the O_2 existing in the O site and the transition metals. [50] The NCM811 cathode with reference electrolytes showed an unclear O-K peak was observed up to 3 nm. (Figure 21c). However, in the TMSP-containing electrolyte, an unclear O-K peak was observed up to about 7 to 8 nm. (Figure 21d). A comparative analysis of X-ray diffraction (XRD) in cathode finished cycles presented the intensity ratio of (003)/(104) ($I_{(003)}/I_{(104)}$) of NCM811 after 200 cycle in the non-containing TMSP (0.397) more higher compared to TMSP-containing electrolyte (0.359). [51] Due to cycling of NCM811 with TMSP was inhibited during delithiation, reducing the discharge capacity of the entire cell. Moreover, when using TMSP on NCM811 cathode, the degree of divisions for (106)/(102) or (108)/(110) was higher (Figure 22c,d). This severe division means alteration to the rock-salt phase. [52] For NCM811 cathode with a TMSP of 0.5%, this result confirms that converted to the rock-salt structure occurred more practically and by reducing the mechanical strength of NCM811 cathode, NCM particles experienced micro-cracking in the process of charging and discharging. To investigate the degradation effect on the cathode electrode when using TMSP, evaluation of the 3D depth TOF-SIMS analysis of some species obtained from NCM811 cathode cycled using 0.5% TMSP presence and non-electrolyte was conducted. The 3D visualization of NCM811 cathode showed an additional strong signal equivalent to P^-, PO_2^- and $PO_2F_2^-$ at TMSP after 200 cycles (Figure 21e). Obviously, PO_2^- peaks were significantly stronger in film of NCM811 cathode at TMSP. $PO_2F_2^-$ peaks were positioned on the CEI surface layer of NCM811 cathode, and LiF_2^- species existed on both the external and bottom of cathode. This data means that the TMSP caused an undesirable chemical decomposition with LiOH at NCM811 and formed phosphorus-rich species over additional breakdown. The result also showed that TMSOH reacts with PF_5 to produce POF_3. $PO_2F_2^-$ was formed through a lateral reaction of POF_3 with a bit amount of H_2O in batteries in Figure 16c. It shows 0.5% TMSP-containing electrolyte has achieved remarkable production of P^-, PO_2^- and PO_2F_2 like on the cathode face while charging and discharging. This unanticipated reaction

encouraged by TMSP additive at Ni-rich cathode is likely to have been further exacerbated by HF attacks and phase conversion, as the uniform CEI has not been established.

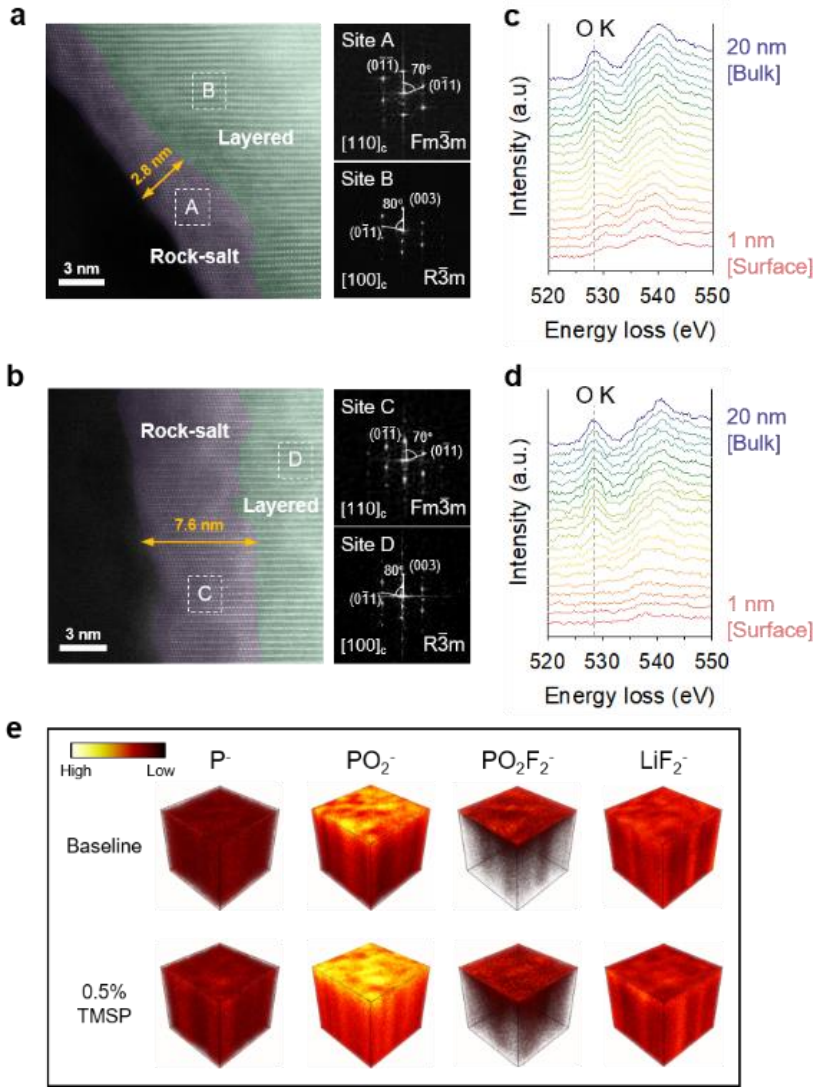

Figure 21. STEM images of the 200 cycled NCM811 cathodes (a) not containing and (b) containing 0.5 wt % TMSP with FFT image. 520 eV – 550 eV range of EELS spectra of (c) baseline electrolyte and (d) 0.5 wt % TMSP-containing electrolyte. (e) 3D depth TOF-SIMS images for species that P^-, PO_2^-, $PO_2F_2^-$ and LiF_2^- ions of NCM811 cathodes of baseline and with 0.5 wt % TMSP electrolyte.

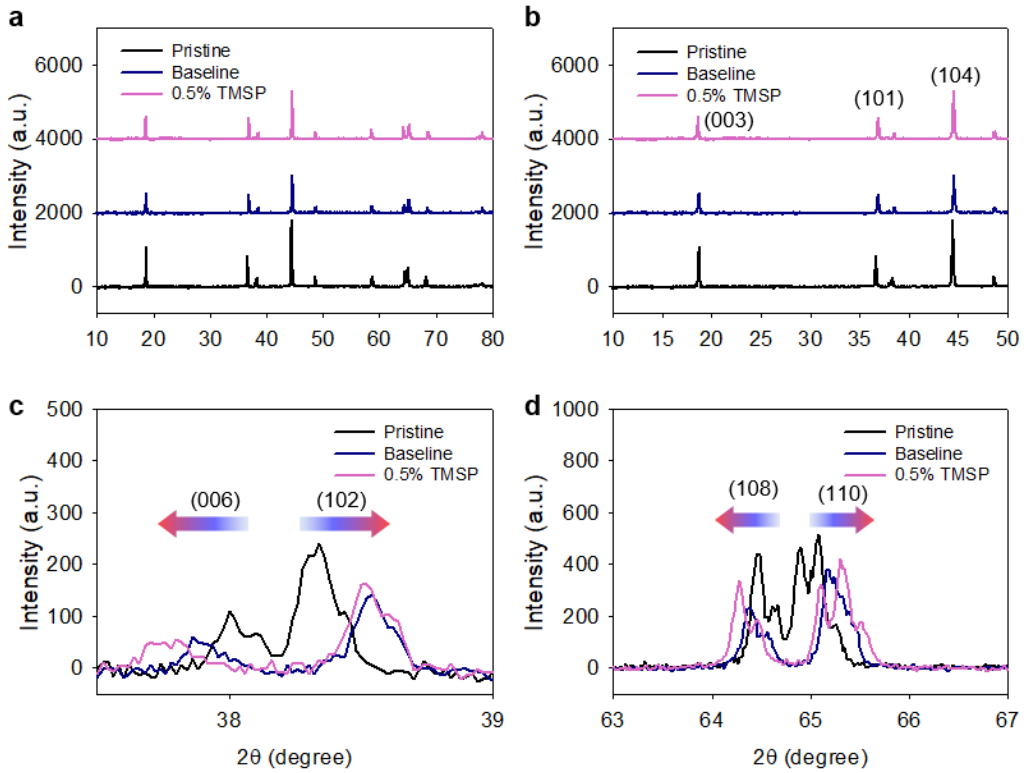

Figure 22. XRD analysis data of the pristine NCM811 cathode and 200 cycled NCM811 cathodes with and without 0.5 wt % TMSP additive in the following 2θ ranges: (a) 10–80°, (b) 10–50°, (c) 37.5–39°, and (d) 63–67°.

Ex-situ-XPS were taken to determine the role of TMSP on the CEI and SEI components. C 1s spectra from NCM811 cathode in TMSP-added electrolyte presented -C-H- (284.9 eV), PVDF (286.4 eV), -C-O- (287.2 eV), -O=C-O- (288.6 eV) and PVDF (290.5 eV). F 1s spectral deconvolution to NCM811 cathode at TMSP showed a comparatively big intensity of LiF at 684.9 eV. TMSP failed to successfully remove HF in $LiPF_6$-based electrolyte due to unwanted reactions with LiOH in NCM811, and may have formed LiF in the cathode. Obviously, in Figure 23a, TMSP managed to the construction of P-O derived film, representing the presence of unstable CEI encouraged by TMSP in NCM811 cathode (P 2p). The results confirm that unanticipated decomposition occurred in TMSP between LiOH at the NCM811, resulting in $PO_2F_2^-$ that could make P-rich film through additional decay (Figure 16c). In O 1s and P 2p spectra, the anode with TMSP is covered by a comparatively high proportion of C=O component derived using VC conserved after 200 cycles and SEI species derived from TMSP (Figure 23b). Undoubtedly, TMSP successfully defends graphite anodes with VC additive despite the fact decomposition of $LiPF_6$ in graphite. The F 1s spectrum supports that the Li-F intensity of SEI in the anode with a TMSP is weaker than the LiF signal of graphite without TMSP additive. This probable due to TMSP's contribution to cleaning up the HF that forms LiF in response to Li-ions. XPS results presented that at NCM811 during cycling, TMSP operated the boundary construction of CEI over undesirable responses with residual species as LiOH, and the result also displayed that CEI degraded the cycle performance of the cathode.

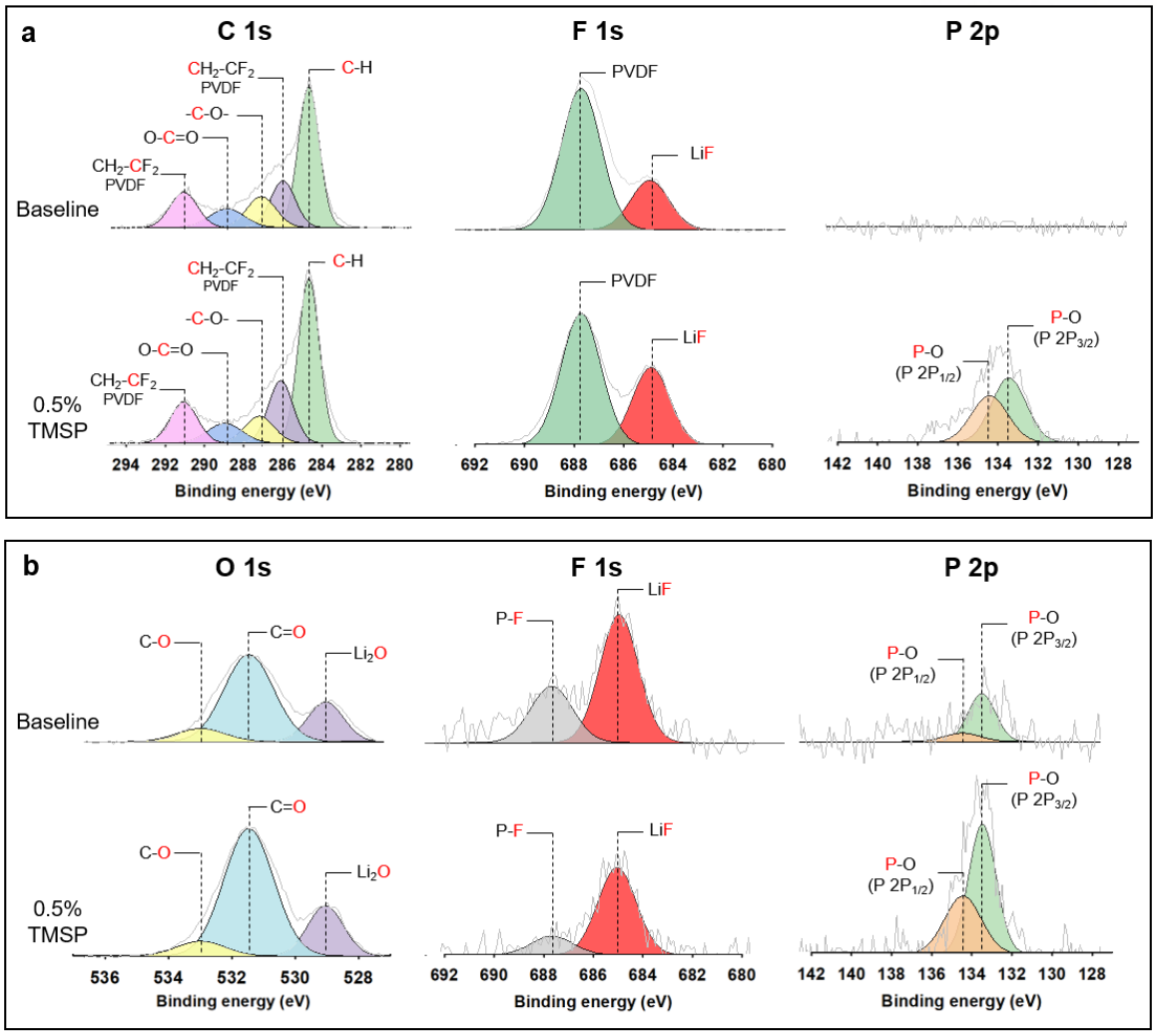

Figure 23. XPS spectra for C 1s, F 1s and P 2p of (a) 200 cycled NCM811 cathodes cycled in baseline electrolytes and 0.5 wt % TMSP-containing electrolyte. O 1s, F 1s and P 2p of (b) 200cycled graphite anodes cycled in baseline electrolyte and 0.5 wt % TMSP.

3. Conclusion

Including TMS moieties, the usage of electrolyte additives, in lithium-ion batteries with NCM811 cathode presented numerous issues, including undesired reactions between residue lithium species, the production of TMSOH from LiOH to cathode producing HF in response to PF_5, and the accumulation of layers of non-uniform interfaces. In particular, HF generated by the reaction between PF_5 and TMSOH can be accelerated with TMSOH. TMSP-induced CEI for NCM811 cathode caused serious micro-cracks of cathode particles by unbalanced charging and discharging reactions and worsened permanent phase changes. From the experiment of surface chemistry of electrodes and probable reactions, we suggested the basic mechanism of electrolyte additives with TMS moiety, which exacerbates the cyclic performance of NCM811 cathode in the cell. My study gives to planning a possible mechanism for battery failure and developing the design of electrolyte additives to figure out well-established CEI or SEI. We offered the usage of electrolyte additives like trimethylsilyl functional groups in lithium-ion full cells with NCM811cathodes has some difficulties, like undesired reactions with residual species, forms TMSOH from lithium hydroxide that reacts with PF_5 to yield CO_2 gas, and the buildup of unfavorable CEI layers in NCM811. Remarkably, HF formed from the reaction between TMSOH and $LiPF_6$-based electrolyte can be removed by TMSOH. Obviously, TMSP-derived interphase motivated micro-cracks on the cathode produced by continuous structural and volume changes through cycling and worsened the irreparable phase transition in the cathode. In XPS and NMR analysis, we planned the fundamental chemical reactions of the electrolyte additive with TMS functional groups degrading the cyclic life span of NCM811 cathode. Our study gives to planning thinkable mechanisms for degradation in batteries and to proceeding the strategy to layout additives to accumulation a safe interface of cathode and anode.

References

[1] I. Belharouak, W. Lu, D. Vissers, and K. Amine, "Safety characteristics of $Li(Ni_{0.8}Co_{0.15}Al_{0.05})O_2$ and $Li(Ni_{1/3}Co_{1/3}Mn_{1/3})O_2$," *Electrochem. commun.*, vol. 8, no. 2, pp. 329–335, Feb. 2006, doi: 10.1016/j.elecom.2005.12.007.

[2] B.-R. Lee, H.-J. Noh, S.-T. Myung, K. Amine, and Y.-K. Sun, "High-Voltage Performance of $LiNi_{0.55}Co_{0.15}Mn_{0.30}O_2$ Positive Electrode Material for Rechargeable Li-Ion Batteries," *J. Electrochem. Soc.*, vol. 158, no. 2, p. A180, Dec. 2011, doi: 10.1149/1.3525247.

[3] J. H. Song *et al.*, "Enhancement of high temperature cycling stability in high-nickel cathode materials with titanium doping," *J. Ind. Eng. Chem.*, vol. 68, pp. 124–128, Dec. 2018, doi: 10.1016/j.jiec.2018.07.036.

[4] T. Ohzuku and Y. Makimura, "Layered lithium insertion material of $LiCo_{1/3}Ni_{1/3}Mn_{1/3}O_2$ for lithium-ion batteries," *Chem. Lett.*, no. 7, pp. 642–643, Feb. 2001, doi: 10.1246/cl.2001.642.

[5] V. Etacheri, R. Marom, R. Elazari, G. Salitra, and D. Aurbach, "Challenges in the development of advanced Li-ion batteries: A review," *Energy and Environmental Science*, vol. 4, no. 9. Royal Society of Chemistry, pp. 3243–3262, 26-Sep-2011, doi: 10.1039/c1ee01598b.

[6] C. Liu, Z. G. Neale, and G. Cao, "Understanding electrochemical potentials of cathode materials in rechargeable batteries," *Materials Today*, vol. 19, no. 2. Elsevier B.V., pp. 109–123, 01-Mar-2016, doi: 10.1016/j.mattod.2015.10.009.

[7] M. M. Doeff, "Batteries: Overview of Battery Cathodes," *Lawrence Berkeley National Laboratory*, 01-Feb-2011. [Online]. Available: https://escholarship.org/uc/item/1n55870s. [Accessed: 28-Nov-2020].

[8] J. H. Kim, K. J. Park, S. J. Kim, C. S. Yoon, and Y. K. Sun, "A method of increasing the energy density of layered High nickel $Li[Ni_{1-2:x}Co_xMn_x]O_2$ cathodes (x = 0.05, 0.1, 0.2)," *J. Mater. Chem. A*, vol. 7, no. 6, pp. 2694–2701, Feb. 2019, doi: 10.1039/c8ta10438g.

[9] J. H. Shim *et al.*, "Effects of heat-treatment atmosphere on electrochemical performances of High nickel mixed-metal oxide ($LiNi_{0.80}Co_{0.15}Mn_{0.05}O_2$) as a cathode material for lithium ion battery," *Electrochim. Acta*, vol. 138, pp. 15–21, Aug. 2014, doi: 10.1016/j.electacta.2014.06.079.

[10] Y. K. Sun, S. T. Myung, M. H. Kim, J. Prakash, and K. Amine, "Synthesis and characterization

of $Li[(Ni_{0.8}Co_{0.1}Mn_{0.1})_{0.8}(Ni_{0.5}Mn_{0.5})_{0.2}]O_2$ with the microscale core-shell structure as the positive electrode material for lithium batteries," *J. Am. Chem. Soc.*, vol. 127, no. 38, pp. 13411–13418, Sep. 2005, doi: 10.1021/ja053675g.

[11] S. S. Zhang, "Problems and their origins of High nickel layered oxide cathode materials," *Energy Storage Mater.*, vol. 24, pp. 247–254, Jan. 2020, doi: 10.1016/j.ensm.2019.08.013.

[12] F. Wu *et al.*, "Improving the reversibility of the H2-H3 phase transitions for layered High nickel oxide cathode towards retarded structural transition and enhanced cycle stability," *Nano Energy*, vol. 59, pp. 50–57, May 2019, doi: 10.1016/j.nanoen.2019.02.027.

[13] J. Xu *et al.*, "Understanding the degradation mechanism of lithium nickel oxide cathodes for Li-ion batteries," *ACS Appl. Mater. Interfaces*, vol. 8, no. 46, pp. 31677–31683, Nov. 2016, doi: 10.1021/acsami.6b11111.

[14] K. Kim, H. Ma, S. Park, and N.-S. Choi, "Electrolyte-Additive-Driven Interfacial Engineering for High-Capacity Electrodes in Lithium-Ion Batteries: Promise and Challenges," *ACS Energy Lett.*, pp. 1537–1553, Apr. 2020, doi: 10.1021/acsenergylett.0c00468.

[15] F. Lin *et al.*, "Surface reconstruction and chemical evolution of stoichiometric layered cathode materials for lithium-ion batteries," *Nat. Commun.*, vol. 5, no. 1, p. 3529, Mar. 2014, doi: 10.1038/ncomms4529.

[16] S. W. Oh, S. H. Park, K. Amine, and Y. K. Sun, "Synthesis and characterization of spherical morphology $[Ni_{0.4}Co_{0.2}Mn_{0.4}]_3O_4$ materials for lithium secondary batteries," *J. Power Sources*, vol. 160, no. 1, pp. 558–562, Sep. 2006, doi: 10.1016/j.jpowsour.2006.01.023.

[17] H. Arai, S. Okada, H. Ohtsuka, M. Ichimura, and J. Yamaki, "Characterization and cathode performance of $Li_{1-x}Ni_{1+x}O_2$ prepared with the excess lithium method," *Solid State Ionics*, vol. 80, no. 3–4, pp. 261–269, Sep. 1995, doi: 10.1016/0167-2738(95)00144-U.

[18] Z. Wang *et al.*, "Passivation of Grain Boundary by Squaraine Zwitterions for Defect Passivation and Efficient Perovskite Solar Cells," *ACS Appl. Mater. Interfaces*, vol. 11, no. 10, pp. 10012–10020, Mar. 2019, doi: 10.1021/acsami.8b22044.

[19] D.-H. Cho *et al.*, " Effect of Residual Lithium Compounds on Layer High nickel $Li[Ni_{0.7}Mn_{0.3}]O_2$," *J. Electrochem. Soc.*, vol. 161, no. 6, pp. A920–A926, Apr. 2014, doi: 10.1149/2.042406jes.

[20] K. Edström, T. Gustafsson, and J. O. Thomas, "The cathode-electrolyte interface in the Li-ion battery," in *Electrochimica Acta*, 2004, vol. 50, no. 2-3 SPEC. ISS., pp. 397–403, doi:

10.1016/j.electacta.2004.03.049.

[21] G. V. Zhuang, G. Chen, J. Shim, X. Song, P. N. Ross, and T. J. Richardson, "Li_2CO_3 in $LiNi_{0.8}Co_{0.15}Al_{0.05}O_2$ cathodes and its effects on capacity and power," *J. Power Sources*, vol. 134, no. 2, pp. 293–297, Aug. 2004, doi: 10.1016/j.jpowsour.2004.02.030.

[22] Y. Kim, "Mechanism of gas evolution from the cathode of lithium-ion batteries at the initial stage of high-temperature storage," *J. Mater. Sci.*, vol. 48, no. 24, pp. 8547–8551, Dec. 2013, doi: 10.1007/s10853-013-7673-2.

[23] J. Kim, H. Lee, H. Cha, M. Yoon, M. Park, and J. Cho, "Prospect and Reality of High nickel Cathode for Commercialization," *Adv. Energy Mater.*, vol. 8, no. 6, p. 1702028, Feb. 2018, doi: 10.1002/aenm.201702028.

[24] X. Zheng *et al.*, "Investigation and improvement on the electrochemical performance and storage characteristics of $LiNiO_2$-based materials for lithium ion battery," *Electrochim. Acta*, vol. 191, pp. 832–840, Feb. 2016, doi: 10.1016/j.electacta.2016.01.142.

[25] S. Liu, H. Wu, L. Huang, M. Xiang, H. Liu, and Y. Zhang, "Synthesis of $Li_2Si_2O_5$-coated $LiNi_{0.6}Co_{0.2}Mn_{0.2}O_2$ cathode materials with enhanced high-voltage electrochemical properties for lithium-ion batteries," *J. Alloys Compd.*, vol. 674, pp. 447–454, Jul. 2016, doi: 10.1016/j.jallcom.2016.03.060.

[26] J. Kim, Y. Hong, K. S. Ryu, M. G. Kim, and J. Cho, "Washing effect of a $LiNi_{0.83}Co_{0.15}Al_{0.02}O_2$ cathode in water," *Electrochem. Solid-State Lett.*, vol. 9, no. 1, p. A19, Nov. 2006, doi: 10.1149/1.2135427.

[27] Y. You, H. Celio, J. Li, A. Dolocan, and A. Manthiram, "Modified High-Nickel Cathodes with Stable Surface Chemistry Against Ambient Air for Lithium-Ion Batteries," *Angew. Chemie Int. Ed.*, vol. 57, no. 22, pp. 6480–6485, May 2018, doi: 10.1002/anie.201801533.

[28] K. Park and B. Choi, "Requirement of high lithium content in High nickel layered oxide material for Li ion batteries," *J. Alloys Compd.*, vol. 766, pp. 470–476, Oct. 2018, doi: 10.1016/j.jallcom.2018.06.135.

[29] R. Jung, M. Metzger, F. Maglia, C. Stinner, and H. A. Gasteiger, " Oxygen Release and Its Effect on the Cycling Stability of $LiNi_xMn_yCo_zO_2$ (NMC) Cathode Materials for Li-Ion Batteries ," *J. Electrochem. Soc.*, vol. 164, no. 7, pp. A1361–A1377, May 2017, doi: 10.1149/2.0021707jes.

[30] G. Sun *et al.*, "The effect of cation mixing controlled by thermal treatment duration on the electrochemical stability of lithium transition-metal oxides," *Phys. Chem. Chem. Phys.*, vol. 19,

no. 44, pp. 29886–29894, Nov. 2017, doi: 10.1039/c7cp05530g.

[31] H. H. Ryu, K. J. Park, C. S. Yoon, and Y. K. Sun, "Capacity fading of high nickel $Li[Ni_xCo_yMn_{1-x-y}]O_2$ ($0.6 \leq x \leq 0.95$) Cathodes for High-Energy-Density Lithium-Ion Batteries: Bulk or Surface Degradation?," *Chem. Mater.*, vol. 30, no. 3, pp. 1155–1163, Feb. 2018, doi: 10.1021/acs.chemmater.7b05269.

[32] W. Liu *et al.*, "Nickel-Rich Layered Lithium Transition-Metal Oxide for High-Energy Lithium-Ion Batteries," *Angew. Chemie Int. Ed.*, vol. 54, no. 15, pp. 4440–4457, Apr. 2015, doi: 10.1002/anie.201409262.

[33] J. G. Han, S. J. Lee, J. Lee, J. S. Kim, K. T. Lee, and N. S. Choi, "Tunable and robust phosphite-derived surface film to protect lithium-rich cathodes in lithium-ion batteries," *ACS Appl. Mater. Interfaces*, vol. 7, no. 15, pp. 8319–8329, Apr. 2015, doi: 10.1021/acsami.5b01770.

[34] Y. M. Song, C. K. Kim, K. E. Kim, S. Y. Hong, and N. S. Choi, "Exploiting chemically and electrochemically reactive phosphite derivatives for high-voltage spinel $LiNi_{0.5}Mn_{1.5}O_4$ cathodes," *J. Power Sources*, vol. 302, pp. 22–30, Jan. 2016, doi: 10.1016/j.jpowsour.2015.10.043.

[35] J. G. Han, K. Kim, Y. Lee, and N. S. Choi, "Scavenging Materials to Stabilize $LiPF_6$-Containing Carbonate-Based Electrolytes for Li-Ion Batteries," *Advanced Materials*, vol. 31, no. 20. Wiley-VCH Verlag, p. 1804822, 17-May-2019, doi: 10.1002/adma.201804822.

[36] K. Kim *et al.*, "Cyclic Aminosilane-Based Additive Ensuring Stable Electrode–Electrolyte Interfaces in Li-Ion Batteries," *Adv. Energy Mater.*, vol. 10, no. 15, p. 2000012, Apr. 2020, doi: 10.1002/aenm.202000012.

[37] D. R. Gallus, R. Wagner, S. Wiemers-Meyer, M. Winter, and I. Cekic-Laskovic, "New insights into the structure-property relationship of high-voltage electrolyte components for lithium-ion batteries using the pKa value," *Electrochim. Acta*, vol. 184, pp. 410–416, Dec. 2015, doi: 10.1016/j.electacta.2015.10.002.

[38] Y. K. Han, J. Yoo, and T. Yim, "Distinct Reaction Characteristics of Electrolyte Additives for High-Voltage Lithium-Ion Batteries: Tris(trimethylsilyl) Phosphite, Borate, and Phosphate," *Electrochim. Acta*, vol. 215, pp. 455–465, Oct. 2016, doi: 10.1016/j.electacta.2016.08.131.

[39] Weishan, "An Unpredictable Hazard in Lithium-ion Batteries from Transition Metal Ions: Dissolution from Cathodes, Deposition on Anodes and Elimination Strategies," *J. Electrochem. Soc*, vol. 167, no. 9, pp. 090514, Apr. 2020, doi: 10.1149/1945-7111/ab847f.

[40] Y.-K. Han, J. Yoo, and T. Yim, "Why is tris(trimethylsilyl) phosphite effective as an additive for high-voltage lithium-ion batteries?," *J. Mater. Chem. A*, vol. 3, no. 20, pp. 10900–10909, 2015, doi: 10.1039/C5TA01253H.

[41] X. Qi *et al.*, "Lifetime limit of tris(trimethylsilyl) phosphite as electrolyte additive for high voltage lithium ion batteries," *RSC Adv.*, vol. 6, no. 44, pp. 38342–38349, Apr. 2016, doi: 10.1039/c6ra06555d.

[42] N. S. Choi, J. G. Han, S. Y. Ha, I. Park, and C. K. Back, "Recent advances in the electrolytes for interfacial stability of high-voltage cathodes in lithium-ion batteries," *RSC Advances*, vol. 5, no. 4. Royal Society of Chemistry, pp. 2732–2748, 08-Dec-2015, doi: 10.1039/c4ra11575a.

[43] L. A. Wessjohann and M. A. Dessoy, "An efficient method for the preparation of silyl esters of diphosphoric, phosphoric, and phosphorous acid," *Polyhedron*, vol. 70, pp. 133–137, Mar. 2014, doi: 10.1016/j.poly.2013.12.024.

[44] T. Yim *et al.*, "5V-class high-voltage batteries with over-lithiated oxide and a multi-functional additive," *J. Mater. Chem. A*, vol. 3, no. 11, pp. 6157–6167, Mar. 2015, doi: 10.1039/c4ta06531j.

[45] S. Dalavi, M. Xu, B. Ravdel, L. Zhou, and B. L. Lucht, "Nonflammable Electrolytes for Lithium-Ion Batteries Containing Dimethyl Methylphosphonate," *J. Electrochem. Soc.*, vol. 157, no. 10, p. A1113, Aug. 2010, doi: 10.1149/1.3473828.

[46] Y. M. Song, J. G. Han, S. Park, K. T. Lee, and N. S. Choi, "A multifunctional phosphite-containing electrolyte for 5 V-class $LiNi_{0.5}Mn_{1.5}O_4$ cathodes with superior electrochemical performance," *J. Mater. Chem. A*, vol. 2, no. 25, pp. 9506–9513, Jul. 2014, doi: 10.1039/c4ta01129e.

[47] S. H. Lim, W. Cho, Y. J. Kim, and T. Yim, "Insight into the electrochemical behaviors of 5V–class high–voltage batteries composed of lithium–rich layered oxide with multifunctional additive," *J. Power Sources*, vol. 336, pp. 465–474, Dec. 2016, doi: 10.1016/j.jpowsour.2016.11.002.

[48] F. Lin *et al.*, "Surface reconstruction and chemical evolution of stoichiometric layered cathode materials for lithium-ion batteries," *Nat. Commun.*, vol. 5, p. 3529, 2014, doi: 10.1038/ncomms4529.

[49] J. Kim *et al.*, "Self-Induced Concentration Gradient in Nickel-Rich Cathodes by Sacrificial Polymeric Bead Clusters for High-Energy Lithium-Ion Batteries," *Adv. Energy Mater.*, vol. 7, no. 12, p. 1602559, Jun. 2017, doi: 10.1002/aenm.201602559.

[50] B. Xu, C. R. Fell, M. Chi, and Y. S. Meng, "Identifying surface structural changes in layered Li-excess nickel manganese oxides in high voltage lithium ion batteries: A joint experimental and theoretical study," *Energy Environ. Sci.*, vol. 4, no. 6, pp. 2223–2233, Jun. 2011, doi: 10.1039/c1ee01131f.

[51] Y. Sun, Y. Zhou, L. Zhang, Y. Shen, and J. Zeng, "Preparation and characterization of lithium-rich ternary cathode materials using novel chelating agent and solvent," *J. Alloys Compd.*, vol. 723, pp. 1142–1149, Nov. 2017, doi: 10.1016/j.jallcom.2017.06.114.

[52] K. Qian *et al.*, "Abuse tolerance behavior of layered oxide-based Li-ion battery during overcharge and over-discharge," *RSC Adv.*, vol. 6, no. 80, pp. 76897–76904, Aug. 2016, doi: 10.1039/c6ra11288a.